Femtosecond phase spectroscopy by use of frequency-domain interference

Eiji Tokunaga* **and Akira Terasaki†**

Department of Physics, Faculty of Science, University of Tokyo, 7-3-1 Hongo, Bunkyo-ku, Tokyo 113, Japan

Takayoshi Kobayashi

Department of Physics, Faculty of Science, University of Tokyo, 7-3-1 Hongo, Bunkyo-ku, Tokyo 113, Japan, and Frontier Research Program, The Institute of Physical and Chemical Research (RIKEN), 2-1 Hirosawa, Wako, Saitama 351-01, Japan

Received March 15, 1994; revised manuscript received October 17, 1994

We present the principles, experimental procedures, applications, and theoretical analyses of femtosecond phase spectroscopy, which is complementary to femtosecond absorption spectroscopy. In femtosecond phase spectroscopy difference spectra of both phase and transmission are simultaneously measured with a frequency-domain interferometer, which is only slightly modified from the conventional pump–probe method. Femtosecond time-resolved dispersion relations for CdS_xSe_{1-x}-doped glass and CS_2 are obtained with transform-limited pulses of 60-fs duration and 620-nm center wavelength. The results are theoretically analyzed and are well reproduced by numerical simulations. Although time-resolved data are not expected to satisfy the Kramers–Kronig (K–K) relations, the degree of discrepancy from the K–K relations is more substantial for CS_2 than for CdS_xSe_{1-x}-doped glass. These results arise from the difference in the linear susceptibility and in the excited-population dynamics. The conditions for which the K–K relations are applicable to time-resolved spectra are obtained theoretically and verified experimentally. It is shown that induced amplitude and phase modulations of the probe pulses cause a deviation from the K–K relations.

1. INTRODUCTION

Time-resolved spectroscopy is one of the new fields in optical spectroscopy that developed along with the advent of the coherent optical pulse source, i.e., the mode-locked pulse laser. Recent advances in short-pulse lasers of high repetition rate and stable operation are remarkable, as represented by the Ti:sapphire laser, so that time-resolved spectroscopy even in the femtosecond regime is more and more popular and is increasing in importance. In particular, to reveal details of ultrashort transient phenomena in optically excited states, femtosecond absorption spectroscopy by a pump–probe method makes powerful contributions because the spectral dependence of transmission changes, the difference transmission spectrum (DTS), can be obtained with a single measurement by use of a white-light continuum pulse and a multichannel spectrometer without the scanning of a probe wavelength. A DTS is usually obtained as the normalized transmission change $\Delta T/T(\omega, \tau)$, where ω is the angular frequency and τ is the time delay between pump and probe pulses.

Absorption spectroscopy offers information not about the real part of the susceptibility change but only about the imaginary part. One method for obtaining the real part is the application of the Kramers–Kronig (K–K) relations,[1,2] which connect the real and the imaginary parts of the linear susceptibility. Even for a nonlinear change of the susceptibility, the extended relations apply[3–6] if the causality condition is satisfied for a response function. Because the K–K relations are also formulated between absorption and reflection spectra, they have frequently been applied to highly absorptive materials, through which no detectable light is transmitted, to permit deduction of transient absorption spectra from transient reflection spectra.[7] However, some ambiguity always remains in application of K–K relations because of the limited spectral range, and an even more serious problem is that no general relations exist in time-resolved spectroscopy because the causality condition is not satisfied.[8] Hence a direct measurement of the phase change is necessary for assessment of the real part of the susceptibility change in time-resolved spectroscopy.

To yield time-resolved phase information, an interferometric technique is combined with the pump–probe method. For this purpose time-resolved interferometry has been a frequently applied methodology, and there have been continuous efforts to develop a novel time-resolved interferometer. Previously many methods were proposed for time-resolved measurement of the phase change,[9–15] but nothing had been comparable with pump–probe spectroscopy, by which the phase change should be both wavelength and time resolved to give a difference phase spectrum (DPS) $\Delta\Phi(\omega, \tau)$ with a single measurement as for a DTS. Simultaneous measurement of the real and the imaginary parts of the optical nonlinearity is also of much importance,[16–18] but we are aware of no measurement of both parts that was both wavelength and time resolved. It has been questioned how one could achieve such measurements.

Time-resolved interferometers that were developed previously[9–15] use spatial interference fringes, which ap-

0740-3224/95/050753-19$06.00

pear as a function of position, x, with a period of $2\pi/\Delta k$, where Δk is the difference in wave number between two light beams. For spatial interference to be observed, temporal coincidence is required between reference and probe pulses from the same light source within the coherence time. Since the coherence time is equal to the pulse duration in the case of transform-limited pulses from a mode-locked laser, the experimental alignment becomes extremely difficult when ultrashort pulses are used. In particular, for pulses with a large bandwidth covering the whole visible region, i.e., for femtosecond white-light continuum pulses, the coherence length is as short as a few wavelengths of visible light, so that the resultant spatial interference pattern consists of only a few fringes. More precisely, each wavelength component of white light makes fringes whose spacing varies with wavelength, resulting in a zeroth-order white central peak and first-order fringes with a continuously changing interference color. This fringe structure is not appropriate for fringe-shift detection.

The wavelength dependence of the phase change can be determined even by spatial interference if a tunable laser or spectral filtering of a continuum is employed. However, such a measurement requires not only a complicated experimental setup but also a long measuring time in that one wavelength after another is measured at each delay position. Furthermore, it does not give a DPS that is the exact counterpart of the DTS obtained with femtosecond continuum pulses and a multichannel spectrometer, because the time resolution is reduced by the narrowed spectral width of the probe.

To overcome the difficulties mentioned above, in a previous Letter[19] we introduced a frequency-domain interferometer (FDI) for femtosecond phase spectroscopy. In contrast to the previous interferometers, the FDI gives a DPS that is the counterpart of the DTS without the need for a complicated experimental arrangement. Furthermore, the FDI realizes a simultaneous measurement of DPS and DTS with a femtosecond time resolution. All these outstanding performances are achieved by use of frequency-domain interference instead of spatial interference. By analogy with beating, which is time-domain interference between two frequency components, frequency-domain interference is produced by two time components, i.e., reference and probe pulses, and appears as a function of angular frequency, ω, with a period of $2\pi/\Delta t$, where Δt is the time separation between the two pulses. In marked contrast to spatial interference, therefore, frequency-domain interference can take place even when the two pulses are spaced by more than the pulse duration, so that the pulse-overlap condition that is necessary in space-domain interference is fully obviated. For the sake of this advantage, for example, frequency-domain interference was previously used for producing a phase-locked pulse pair to excite vibronic transitions of a molecule coherently.[20]

In previous short reports we proposed the FDI[19] and demonstrated the breakdown of the K–K relations in time-resolved spectroscopy.[8] In this paper the complicated features of the DTS and the DPS obtained by the FDI are theoretically analyzed, together with a full description of the method. The experimental results are compared with the K–K relations to give a practical guide for application of the K–K relations in time-resolved spectroscopy.

This paper is organized as follows. In Section 2 the principle of the method and the experimental procedure are described. In Section 3 the experimental results and their numerical analyses are presented. In Section 4 the applicability of the K–K relations in time-resolved spectroscopy is discussed, and the experimental results are compared with the K–K relations. In Section 5 the results of the paper are summarized.

2. EXPERIMENTAL METHODS

A. Experimental Setup

The laser source, which was described in detail elsewhere,[21] is a standard combination of a colliding-pulse mode-locked ring dye laser and a six-pass amplifier pumped by a copper-vapor laser, generating pulses of 620-nm wavelength, 60-fs duration, 2-μJ pulse energy, and 10-kHz repetition rate.

The schematic of the FDI apparatus is shown in Fig. 1(a).[19] The pulse is divided into three parts, i.e., pump, probe, and reference pulses. The probe is delayed from the pump by τ with a variable delay line. At a Michelson interferometer the reference and the probe are displaced by T for frequency-domain interferometry by adjustment of the arm length. To avoid the effect of the pump on the reference, one sets the displacement T in such a way that the reference arrives at the sample earlier than both pump and probe. The three pulses are focused into the sample, with the pump and the probe beams making a small angle and the reference and the probe beams being collinear. The spectrum of the transmitted reference and probe pulses is detected through

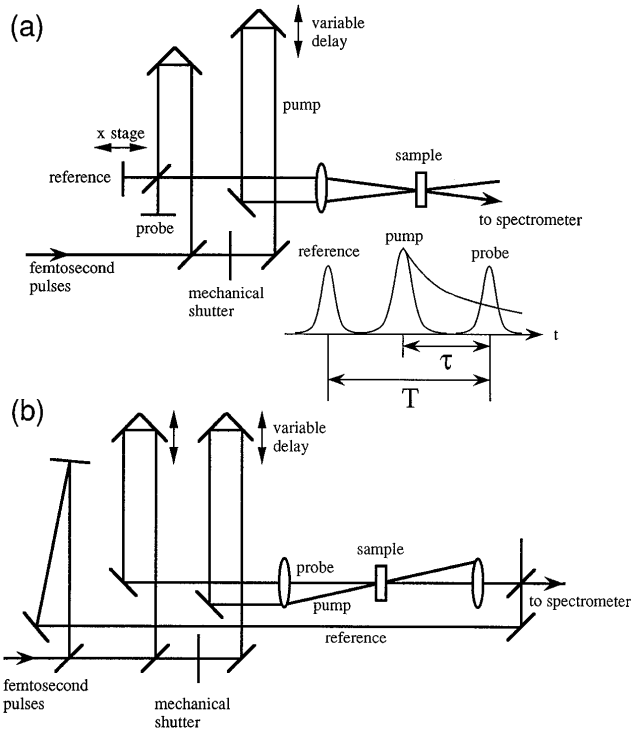

Fig. 1. (a) Experimental setup of the FDI and the time sequence of pump, probe, and reference pulses with separations τ and T. (b) Another possible setup of the FDI that is suited to measurements at time delays longer than T.

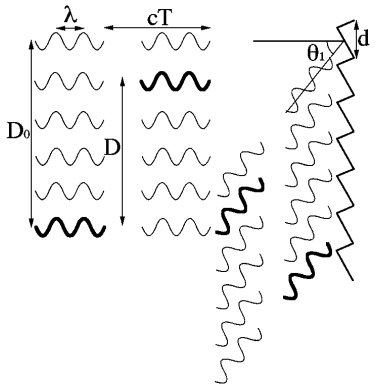

Fig. 2. Mechanism of frequency-domain interference by a grating. θ_1 is the first-order diffraction angle, d is the period of the grating grooves, D_0 is the transverse dimension of the pulses, and D is the transverse distance between the pair of components that make the largest contribution to interpulse interference. See text for details.

a spectrometer with a multichannel photodiode array. With the pump beam blocked with a mechanical shutter at ~5 Hz, the spectra with and without excitation are taken alternately to yield the difference spectra as a function of time delay τ with displacement T fixed throughout the delay changes. With the reference beam blocked, the ordinary pump–probe measurement can be performed to yield the DTS.

B. Principle of the Method

How the above method gives the DPS is explained as follows. The probe and the reference pulses temporally displaced by T are expressed as[22]

$$E_{\mathrm{pr}}(t) = E(t)\exp(i\omega_0 t),$$
$$E_{\mathrm{ref}}(t) = E(t+T)\exp[i\omega_0(t+T)], \tag{1}$$

where ω_0 is a central angular frequency and $E(t)$ is generally a complex function. In the frequency domain the two pulses are expressed by the Fourier transform (FT) as

$$F[E_{\mathrm{pr}}(t) + E_{\mathrm{ref}}(t)] = E(\omega-\omega_0)[1+\exp(i\omega T)], \tag{2}$$

where $E(\omega) \equiv F[E(t)]$. Experimentally obtained is the power spectrum:

$$|F[E_{\mathrm{pr}}(t) + E_{\mathrm{ref}}(t)]|^2 = |E(\omega-\omega_0)|^2(2+2\cos\omega T), \tag{3}$$

which represents the frequency-domain interference with the fringe separation of $2\pi/T$.

The optical field of a probe pulse transmitted through a medium in the plane-wave approximation is given by

$$E_{\mathrm{pr}}'(t) = \frac{1}{2\pi}\int \mathrm{d}\omega E(\omega-\omega_0)\exp\{i\omega[t - n_c(\omega)L/c]\}, \tag{4}$$

where L is the thickness of the medium, c is the velocity of light in vacuum, and $n_c(\omega)$ is the complex refractive index of the medium defined by $n_c(\omega) \equiv n(\omega) - ik(\omega)$. The FT of Eq. (4) is obtained as follows:

$$E_{\mathrm{pr}}'(\omega) \equiv F[E_{\mathrm{pr}}'(t)] = E(\omega-\omega_0)\exp[-in_c(\omega)\omega L/c]. \tag{5}$$

Since the reference pulse is transmitted through the same medium as the probe, the reference spectrum is given by $E_{\mathrm{ref}}'(\omega) = E(\omega-\omega_0)\exp[i\omega T - in_c(\omega)\omega L/c]$. On excitation of the medium by the pump, only the probe pulse undergoes a change in the complex refractive index, $\Delta n_c(\omega,\tau) \equiv \Delta n(\omega,\tau) - i\Delta k(\omega,\tau)$, such that

$$E_{\mathrm{pr}}'(\omega,\tau) \equiv F[E_{\mathrm{pr}}'(t,\tau)] = E_{\mathrm{pr}}'(\omega)\exp[i\Delta\Phi(\omega,\tau) - \Delta K(\omega,\tau)], \tag{6}$$

where $\Delta\Phi \equiv -\Delta n\omega L/c$ and $\Delta K \equiv \Delta k\omega L/c$. Without the reference pulse the method is reduced to the conventional pump–probe measurement. The DTS[23] is obtained as

$$\Delta T/T(\omega,\tau) = \frac{|E_{\mathrm{pr}}'(\omega,\tau)|^2 - |E_{\mathrm{pr}}'(\omega)|^2}{|E_{\mathrm{pr}}'(\omega)|^2} = \exp[-2\Delta K(\omega,\tau)] - 1. \tag{7}$$

When the change is small, this becomes

$$\Delta T/T(\omega,\tau) \sim -2\Delta K(\omega,\tau) = -\Delta\alpha(\omega,\tau)L, \tag{8}$$

where $\Delta\alpha$ is the change in the absorption coefficient α. In this measurement only the imaginary part of Δn_c is obtained. With the reference pulse, on the other hand, the interference signal without excitation is expressed by

$$|E_{\mathrm{pr}}'(\omega) + E_{\mathrm{ref}}'(\omega)|^2 = |E_{\mathrm{pr}}'(\omega)|^2(2+2\cos\omega T), \tag{9}$$

and the interference signal with excitation by

$$|E_{\mathrm{pr}}'(\omega,\tau) + E_{\mathrm{ref}}'(\omega)|^2 = |E_{\mathrm{pr}}'(\omega)|^2\{1+\exp[-2\Delta K(\omega,\tau)] + 2\exp[-\Delta K(\omega,\tau)] \times \cos[\omega T - \Delta\Phi(\omega,\tau)]\}. \tag{10}$$

Comparing Eq. (10) with Eq. (9), we see that $\Delta\Phi(\omega,\tau)$ and $\Delta K(\omega,\tau)$ can be simultaneously determined from the peak shifts and the amplitude changes of the fringes, respectively, with a multichannel spectrometer.

C. Physical Mechanism of Frequency-Domain Interference

Experimentally time-dependent signals are Fourier transformed by a grating in a spectrometer. In this process temporally separated pulses can interfere with each other because the linear dispersion of a grating broadens the pulse widths[24] to make them overlap temporally, as illustrated in Fig. 2. When light is normally incident upon a grating, it is diffracted at an angle θ such that optical path differences between different transverse components of light are introduced. All the diffracted components interfere constructively at the angle $\theta = \theta_i$, which satisfies

$$d\sin\theta_i = i\lambda, \tag{11}$$

where i is an integer indicating the order of diffraction, d is the period of the grating grooves, and λ is the wavelength of light. Monochromatic light produces δ-function diffraction peaks at $\theta = \theta_1, \theta_2, \ldots$, because even a slight departure from θ_i makes any diffracted component interfere destructively with another component diffracted from a distant groove that has a half-wavelength path difference. A short light pulse, on the other hand, produces finite-width diffraction peaks at θ_i, i.e., a long period of modulation as a function of θ, because the destructive interference is incomplete owing to partial temporal

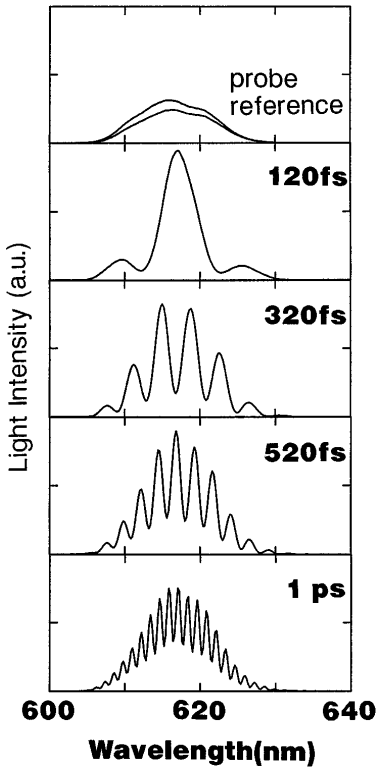

Fig. 3. Frequency-domain interference between the probe and the reference for several time displacements.

overlap between the finite-duration components. Now we consider the first-order diffraction ($i = 1$). For the pulse with a transverse dimension D_0, the pulse duration broadens to $D_0 \sin \theta_1/c$ from Eq. (11). Therefore the two pulses separated by T can interfere if $T \leqq D_0 \sin \theta_1/c$. For simplicity the case of $cT = m\lambda$ with $m = 4$ is illustrated in Fig. 2, but m does not need to be an integer. For interpulse interference the interference between two components that are transversely separated by $D = md$ (thick wavy curves in Fig. 2) gives the largest contribution because of the complete temporal overlap of the two components. The condition for constructive interference between the two components is

$$D \sin \theta_j = j\lambda, \tag{12}$$

where j is an integer. Since $D \gg d$, a shorter period of modulation as a function of θ results from Eq. (12) than from Eq. (11). This represents the frequency domain interference.

Figure 3 shows frequency-domain interference obtained for several values of the time displacement between the reference and the probe, T. The visibility of the fringes is reduced as T is increased because of the limited wavelength resolution of the system that includes the finite transverse size effect as shown in Fig. 2. The reference and the probe spectra separately measured are shown at the top of Fig. 3, where the intensity of the reference is different from that of the probe as a result of the incomplete spatial overlap. Even with this incomplete alignment, interference was observable for more than $T = 5$ ps (1.5 mm in length). Thus, by monitoring the fringe period as a measure of the time displacement, one can readily find the zero displacement position between the reference and the probe pulses.

D. Advantages of the Frequency-Domain Interferometer

The setup in Fig. 1(a) employs the temporal division scheme[10,14] for separating the reference from the probe. Since there is no need for overlapping the pulses temporally after a sample, the configuration is much simpler than the time-division measurement by LaGasse *et al.*[14] By this setup, for τ longer than T, the signal gives the difference in $\Delta\Phi(\omega, \tau)$ between $\tau - T$ and τ because the reference is also influenced by the pump. The maximum time delay to yield $\Delta\Phi(\omega, \tau)$ itself is limited to T, and T is then limited by the system wavelength resolution. Here the time delay is limited to a few picoseconds by use of a 25-cm spectrometer with 0.2-nm resolution. To extend the time delay range, a spectrometer with higher resolution must be used. Otherwise not a time-division but a space-division configuration must be used, as shown in Fig. 1(b), where the reference and the probe travel along different paths in a Mach–Zehnder interferometer to be spatially overlapped after the sample with time displacement T. However, the setup in Fig. 1(a) is employed here because it is superior to that in Fig. 1(b) in the following respects:

1. The setup of Fig. 1(a) is obtained by the addition of only two more optical components, a beam splitter and a mirror, to the pump–probe setup. This is the simplest configuration of all the time-resolved interferometers developed so far.
2. The optical alignment process is much easier for overlapping the reference and the probe either spatially or temporally in the setup of Fig. 1(a) than in that of Fig. 1(b).
3. The visibility of the interference fringes is higher because both reference and probe pulses are transmitted through the sample to yield the same spectra.
4. It is unnecessary to readjust the optical path difference between the reference and the probe when samples are exchanged. To compensate for disadvantages with respect to factors 3 and 4 for the setup of Fig. 1(b), one must place identical samples in the probe and the reference paths.
5. Since the time-division scheme is employed, the configuration is more stable against path-length fluctuation caused by the oscillations of optical elements. It is also less sensitive to beam deflection, because the path difference between the reference and the probe is only the two short arms of the Michelson interferometer. Hence, we were able to obtain the data with a high signal-to-noise ratio, as is shown below, even though a feedback technique for stabilization was not used.

If setup of Fig. 1(b) is employed, we can set $T = 0$ in Eq. (10) to obtain the spectra:

$$|E_{\mathrm{pr}}'(\omega, \tau) + E_{\mathrm{ref}}'(\omega)|^2 = |E_{\mathrm{pr}}'(\omega)|^2\{1 + \exp[-2\Delta K(\omega, \tau)] + 2\exp[-\Delta K(\omega, \tau)]\cos \Delta\Phi(\omega, \tau)\}. \tag{13}$$

From Eq. (13), if $\Delta K(\omega, \tau)$ is known from the ordinary pump–probe measurement, we can deduce $\Delta\Phi(\omega, \tau)$ without the use of frequency-domain interference. However, it is difficult to stabilize T precisely at zero with the space-division setup of Fig. 1(b). Even a small fluctuation of T around $T = 0$ brings about serious inten-

sity fluctuations in the spectrum as a result of the factor $\cos[\omega T - \Delta\Phi(\omega, \tau)]$, making it difficult to evaluate $\Delta\Phi(\omega, \tau)$ precisely. It is also difficult to determine the sign of $\Delta\Phi(\omega, \tau)$ in the cosine function. In principle it is ideal to obtain the $\sin \Delta\Phi(\omega, \tau)$ dependence by setting $\omega T = \pi/2$, but this is difficult experimentally because the nonlinear chirp must be introduced into the reference pulse.

E. Method of Data Analysis

Figure 4 shows signals observed by the FDI for an R63 glass filter (Toshiba) at $\tau = 20$ fs and $T = 410$ fs [Fig. 4(a)] and for CS_2 at $\tau = -40$ fs and $T = 370$ fs [Fig. 4(b)]. The interference spectra with and without excitation (curves a and b) in the upper panels are the averages over 20 cycles of the pump on and off, taken for 4 s.

The DPS's are given by the open circles in the lower panels. With the normalized interference spectra (curves a′ and b′) the phase shifts are calculated from the ith fringe-valley wavelengths with and without excitation, λ_i^{ex} and λ_i, as

$$\Delta\Phi(\lambda_i) = 2\pi(\lambda_i - \lambda_i^{\text{ex}})/(\lambda_{i+1} - \lambda_i), \tag{14}$$

where $\lambda_{i+1} > \lambda_i$. Because our multichannel spectrometer has a limited resolution (0.2 nm per channel), parabola fitting was employed for determination of a valley wavelength with three data points taken around the valley.

The normalized difference interference spectra (curves c′) show the DTS when the fringe structures are smoothed, because the spectra are calculated by [Eq. (10) − Eq. (9)]/$|E_{\text{pr}}'(\omega)|^2$, which is proportional to Eq. (7) if $\cos \omega T$ terms are ignored. That is, both the DPS and the DTS can be simultaneously measured. In what follows, however, the DTS are separately measured with the reference beam blocked to avoid fringe structures.

The sign of $\Delta\Phi$ depends on the sign of T. Since the reference precedes the probe, $T > 0$ in Eq. (10). Then, if $\Delta\Phi > 0$ (<0), the fringes shift to shorter (longer) wavelengths as in Eq. (14). If spatial interference is used, on the other hand, it is difficult to determine the sign unless a standard sample is used or a path difference is tentatively introduced to allow one to monitor the direction of the fringe shift. This is also one of the advantages of frequency-domain interference.

To calculate the phase shift, we used not fringe peaks but fringe valleys, because the systematic error in $\Delta\Phi$ is caused by the amplitude change ΔK and it is smaller for the valleys. The systematic error is estimated in Appendix A as

$$\Delta\Phi - \Delta\Phi_m \sim \frac{[1 \pm \exp(-\Delta K)]\mathrm{d}\Delta K/\mathrm{d}\omega}{T - \mathrm{d}\Delta\Phi/\mathrm{d}\omega}, \tag{15}$$

where $\Delta\Phi$ and $\Delta\Phi_m$ are true and measured phase shifts, respectively, and + and − correspond to fringe peaks and valleys, respectively. Since $\exp(-\Delta K) > 0$, the fringe valleys cause smaller errors, which are estimated to be less than 0.01 rad for CS_2.[2] For the R63 filter,[1] on the other hand, both $\exp(-\Delta K)$ and $\mathrm{d}\Delta K/\mathrm{d}\omega$ are large near 610 nm, where the errors are estimated to be 0.1 rad at most. Except in the immediate vicinity of 610 nm, however, the errors are negligible compared with the magnitudes of the phase changes. Note that these errors can be reduced by an increase in T.

The phase shifts averaged over the probed spectral region, which are given at the upper right-hand corners of the upper panels of Fig. 4 (0.44 and −0.25 rad), were obtained by Fourier transformation of interference spectra a and b in the upper panels [Eqs. (10) and (9)] into the time domain to make the information for the whole fringes available.[13,15] The detailed procedure is given in Appendix B. As is shown in Appendix B, if $E_{\text{pr}}'(t)$ is an

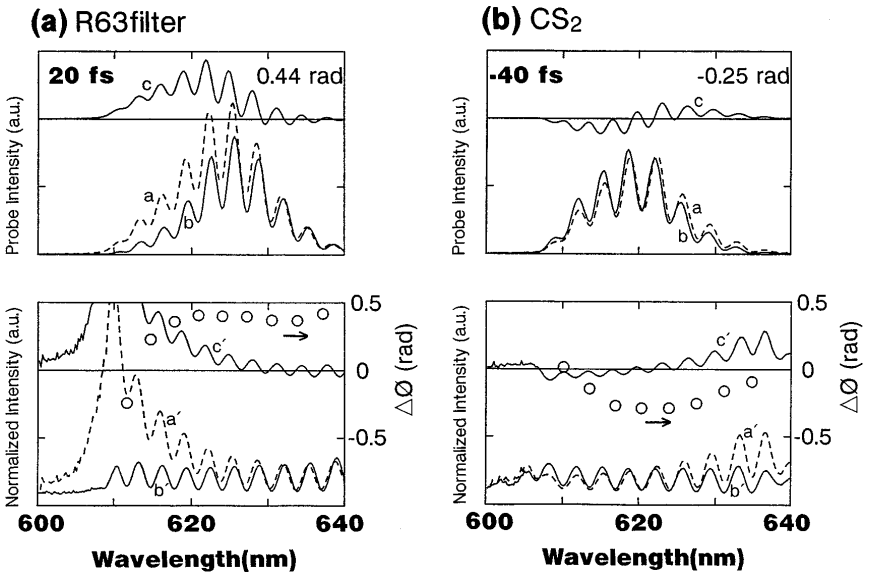

Fig. 4. FDI signals. (a) R63 filter at $\tau = 20$ fs and $T = 410$ fs; (b) CS_2 at $\tau = -40$ fs and $T = 370$ fs. The average phase shifts, (a) 0.44 rad and (b) −0.25 rad, are calculated from the FT. Upper panels, Directly observed interference spectra with excitation (curves a) and without excitation (curves b) and the difference interference spectra (curves c) between them. Lower panels, Curves a, b, and c normalized by the transmitted probe spectra to yield curves a′, b′, and c′, respectively. The open circles (DPS) are calculated from the fringe-valley shifts between curves a′ and b′ as $2\pi(\lambda_i - \lambda_i^{\text{ex}})/(\lambda_{i+1} - \lambda_i)$, where λ_i^{ex} and λ_i are the ith fringe-valley wavelengths with and without excitation, respectively.

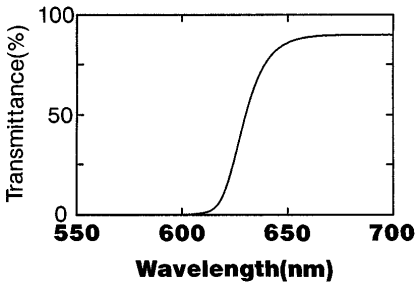

Fig. 5. Transmission spectrum of the R63 filter.

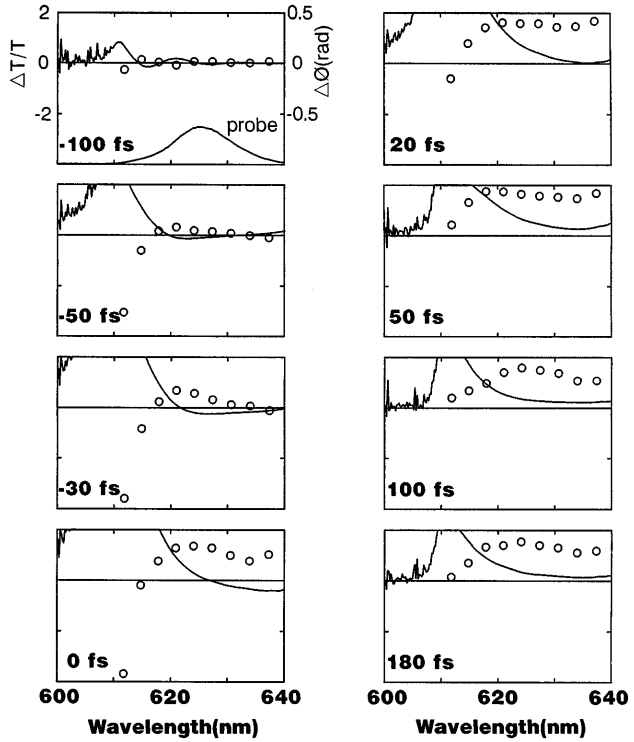

Fig. 6. DTS's (solid curves) and DPS's (open circles) for the R63 filter.

even function, then the Fourier-transformed data give exactly the same values as those obtained by conventional interferometers.

3. RESULTS AND DISCUSSION

To demonstrate the method and to study time-resolved dispersion relations, we have measured two samples, CdS_xSe_{1-x}-doped glass (R63 filter) and CS_2, because they have large nonlinearities and their dynamics have been studied in detail. The polarizations of all the pulses were parallel, and all the experiments were performed at room temperature.

A. CdS_xSe_{1-x}-Doped Glass

The typical results of femtosecond phase spectroscopy were obtained with a Toshiba R63 glass filter[25] containing CdS_xSe_{1-x} microcrystallites of a few weight percent. The pump-pulse energy was 0.3 μJ, and the excitation density was $\sim$3.8 mJ/cm^2. Figure 5 shows the transmission spectrum of the sample, and Fig. 6 shows DTS's and DPS's for several time delays. In Fig. 7 the delay-time dependence of the average phase change is plotted. The average transmission change showed the same dynamics as that of the phase.

In Fig. 8 normalized difference interference spectra and DTS's are plotted together. If the fringe structures are smoothed, the difference interference spectra show good agreement with the DTS's, as expected from the mathematical expressions for the former, [Eq. (10) − Eq. (9)]$/|E_{pr}(\omega)|^2$, and the latter, Eq. (7). This agreement demonstrates that both DTS's and DPS's can be simultaneously measured by the FDI.

At −100 fs, oscillatory behavior is seen in both DTS's and DPS's. The oscillatory structures in DTS's for negative time delays are well known as transient oscillations, which are caused by the coherent coupling effect,[26–30] but the present result was the first observation, to our knowledge, of an oscillating structure in a DPS.[19] From −50 to 0 fs, the absorption saturation grows near 620 nm, accompanied by the negative transmission change for the longer-wavelength side. From the oscillatory features of the DTS at −100 and −50 fs and the fact that the oscillating period of transient oscillations is inversely proportional to the time delay, this negative change should be assigned not to the induced absorption but to transient

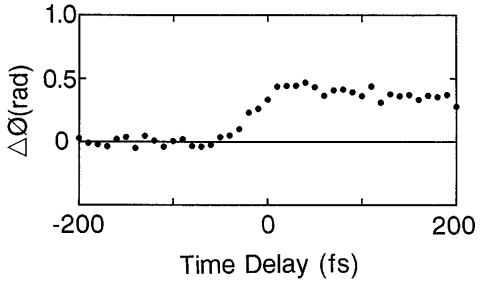

Fig. 7. Delay-time dependence of $\Delta\Phi$ for the R63 filter, derived from the FT of the interference data. $\Delta T/T$ also shows the same dynamics.

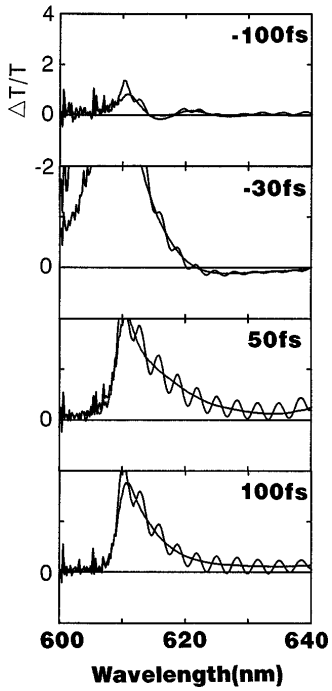

Fig. 8. Normalized difference interference spectra measured with the FDI, and DTS's measured with the reference pulses blocked.

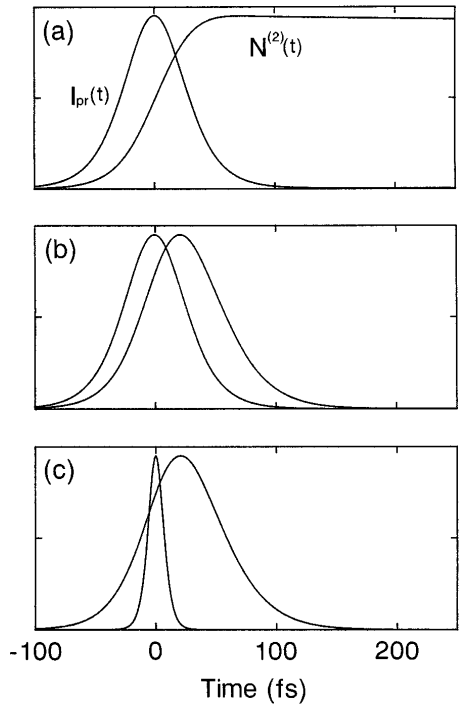

Fig. 9. $I_{pr}(t)$, and $N^{(2)}(t)$, assumed for the calculation in Figs. 10, 13, and 14 below, are shown in (a), (b), and (c), respectively. $I_{pr}(t)$ is placed at delay zero.

oscillations with a longer period. In other words, the signals exhibit blue shifts in the transmitted probe spectra as well as in the absorption saturation. This is evidenced by the rapid rise of the DPS from negative to zero delay, which should cause the induced phase modulation[31–34] (IPM) of the probe pulse. In this process the probe pulse is phase modulated by the rapid change in the refractive index in the medium to yield the frequency shift that is proportional to the time derivative of the phase change. Without the DPS one cannot tell whether the transmission change is due to the absorption change or to the spectral shift of the probe. At 100 and 180 fs both phase and transmission changes decrease from 620 to 640 nm with wavelength, whereas at 20 and 50 fs they increase from 635 nm. Since this behavior can hardly be explained in terms of semiconductor dynamics, it should also be attributed to the transient oscillations with longer periods. For delays longer than 100 fs, both DPS's and DTS's are almost the same as those at 100 fs.

Since both average phase and transmission changes show the same dynamics as a function of τ in Fig. 7, the experimental results for the R63 filter can be numerically simulated by assumption of a two-level system in the first approximation [see Eq. (29) and Note 35]. The third-order nonlinear polarization $P^{(3)}(t)$ in a two-level system for the pump–probe measurement consists of the level-population term and the coherent coupling term.[29] The linear susceptibility $\chi^{(1)}(\omega)$ and the third-order susceptibility $\chi^{(3)}(\omega, \tau)$ that are due to the level-population term are expressed by

$$\chi^{(1)}(\omega) = F[P^{(1)}(t)]/E_{pr}(\omega) = 2\mu N_0 f_2(\omega), \tag{16}$$

$$\chi^{(3)}(\omega, \tau) = F[P^{(3)}(t)]/E_{pr}(\omega) = 2\mu f_2(\omega) F[E_{pr}(t) N^{(2)}(t)]/E_{pr}(\omega), \tag{17}$$

where μ is the transition dipole moment; N_0 is the equilibrated population difference; $f_2(\omega)$ is the FT of the response function $f_2(t)$, which decays with phase relaxation time T_2; and $N^{(2)}$ is the second-order population-difference change. The details of the derivation of Eqs. (16) and (17) are given in Appendix C.

The coherent term, which is further decomposed into the pump-polarization-coupling term and the perturbed free-induction-decay term,[29] was also calculated but is not shown here because it makes little qualitative difference for the following two reasons: First, since the same pulses are used for both the pump and the probe, the coherent coupling term is equivalent to the level population term at zero delay. Second, since the phase relaxation time of the Toshiba R63 filter is much shorter than the pulse duration,[36] the coherent coupling effect is not significant, except for delays shorter than the pulse duration.

Figure 9(a) shows the assumed temporal dynamics of $N^{(2)}(t)$ and $I_{pr}(t)$ at zero delay, and Fig. 10 shows the results of the numerical calculation of Eqs. (16) and (17) with the following parameters:

$$T_1 = 10 \text{ ps}, \quad T_2 = 30 \text{ fs}, \quad \tau_{pr} = \tau_{ex} = 60 \text{ fs},$$
$$\Lambda(=2\pi c/\Omega) = 610 \text{ nm},$$
$$\lambda_{pr}(=2\pi c/\omega_{pr}) = 620 \text{ nm}, \quad \lambda_{ex}(=2\pi c/\omega_{ex}) = 620 \text{ nm},$$

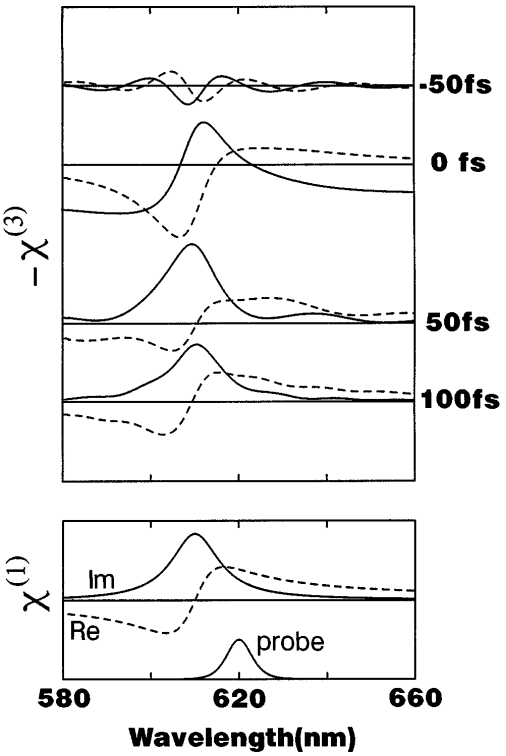

Fig. 10. Results of the simulation for the R63 filter. Upper part, Real (dashed curves) and imaginary (solid curves) parts of $\chi^{(3)}(\omega, \tau)$ calculated from Eq. (17) for the condition $T_2 < \tau_{pr} = \tau_{ex} < T_1$ ($T_1 = 10$ ps, $T_2 = 30$ fs, $\tau_{pr} = \tau_{ex} = 60$ fs, $\Lambda = 610$ nm, and $\lambda_{pr} = \lambda_{ex} = 620$ nm). The assumed temporal dynamics is displayed in Fig. 9(a). -2 Im $\chi^{(3)}$ and $-$Re $\chi^{(3)}$ correspond to the DTS's and the DPS's, respectively. These results reproduce the qualitative features of the experimental results shown in Fig. 6. Lower part, $\chi^{(1)}(\omega)$ and the probe spectrum.

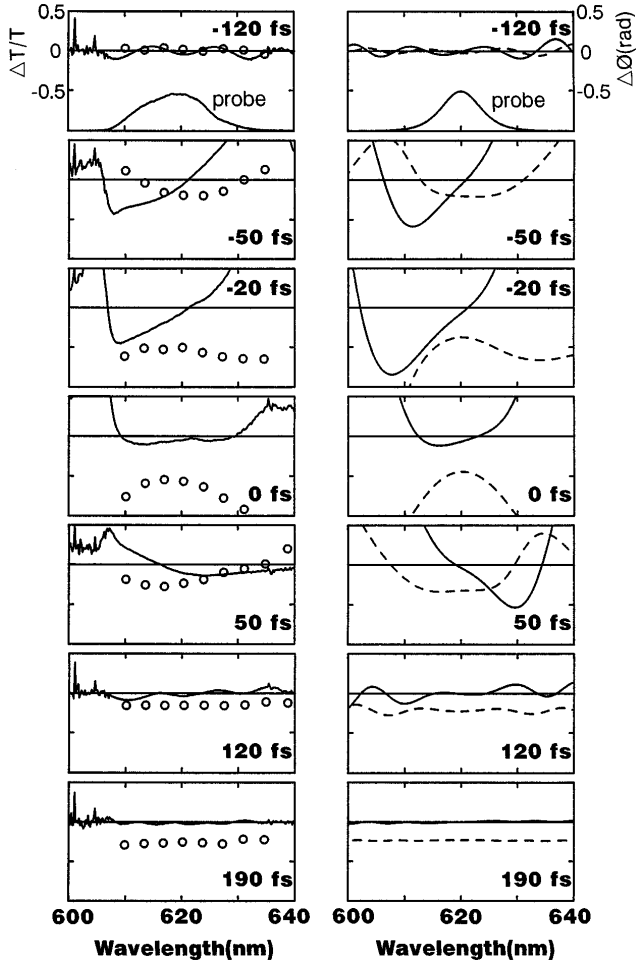

Fig. 11. Left-hand plots, Experimental results for CS_2. Solid curves, DTS; open circles, DPS. Right-hand plots, Results of the simulation from Eqs. (20) and (21). Solid curves, DTS; dashed curves, DPS.

where $T_{1,2}$ are the energy and phase relaxation times, $\tau_{ex,pr}$ are the FWHM's of the pump and the probe intensities, $\omega_{ex,pr}$ are the pump and the probe frequencies, and Ω is the transition frequency. Here we made the reasonable assumptions for this material that the energy relaxation time is much longer ($T_1 = 10$ ps) and the phase relaxation time shorter ($T_2 = 30$ fs) than the pulse duration and that the excitation is off resonant. Since the real and the imaginary parts of $\chi^{(3)}(\omega, \tau)$ are proportional to the DPS and the DTS, respectively, as $\Delta\Phi \propto -\mathrm{Re}\ \chi^{(3)}$ and $\Delta T/T \propto -2\ \mathrm{Im}\ \chi^{(3)}$, the results in Fig. 10 satisfactorily reproduce the typical features of the experimental results shown in Fig. 6.

The reason that the approximation of a two-level system works well is attributed to the band-edge excitation. The absorption saturation at the band edge relaxes only by interband relaxation. As a result the saturation spectrum does not change in shape but changes only in magnitude with the time delay, which is similar to the saturation relaxation in a two-level system. Hence, if the excitation is deeper into the band than in the present experiment, such a simple approximation may not be used.

In Fig. 10, compared with $\chi^{(1)}(\omega)$, $\chi^{(3)}(\omega, \tau)$ exhibits characteristic oscillatory behavior. This is explained by the following equation:

$$\chi^{(3)}(\omega, \tau) = \chi^{(1)}(\omega) F[E_{pr}(t)N^{(2)}(t)]/(E_{pr}(\omega)N_0), \quad (18)$$

which is obtained by substitution of Eq. (16) into Eq. (17). This shows that $\chi^{(3)}(\omega, \tau)$ is different from $\chi^{(1)}(\omega)$ by a factor of $F[E_{pr}(t)N^{(2)}(t)]/(E_{pr}(\omega)N_0)$. Since $N^{(2)}(t)$ depends on τ such that $N^{(2)}(t) = N^{(2)\prime}(t + \tau)$ [$N^{(2)}(\omega) = \exp(i\omega\tau)N^{(2)\prime}(\omega)$], Eq. (18) can also be expressed as

$$\chi^{(3)}(\omega, \tau) = \chi^{(1)}(\omega) \frac{\exp(i\omega\tau)}{E_{pr}(\omega)N_0} \int d\omega' E_{pr}(\omega') \times \exp(-i\omega'\tau)N^{(2)\prime}(\omega - \omega'). \quad (19)$$

The oscillatory behavior is attributed to the $F[E_{pr}(t)N^{(2)}(t)]/(E_{pr}(\omega)N_0)$ factor in Eq. (18) or the $\exp(i\omega\tau)$ factor in Eq. (19). This factor represents induced modulation effects; as discussed in Ref. 34, the transient oscillations by the level-population term are due to the induced amplitude modulation (IAM) and IPM of the probe pulse. The negative transmission change near zero delay is well reproduced by the simulation. Since we assumed the two-level system in which excited-state absorption is forbidden, the negative change is unequivocally attributed to the pulse-modulation effects. All the other nontrivial features in Fig. 6 are also well reproduced by the simulation, so that they are attributed to part of the transient oscillations with longer periods.

Because of the limited spectral range, quantitative evaluation of the K–K relations cannot be performed, but at least it can be stated that the results in Figs. 6 and 10 qualitatively satisfy the K–K relations: The negative absorption change near 610 nm is accompanied by the negative refractive-index change for the longer-wavelength side. However, from the fact that the spectral shift that is due to IPM depends not on the phase itself but on the changing rate of the phase, it is suggested that the K–K relations are not satisfied in Fig. 6. A close link is expected between the pulse-modulation effects and the breakdown of the K–K relations. This is more clearly seen in the results for CS_2, discussed in the next subsection.

B. CS_2

In the case of absorptive materials, it is difficult to discriminate between the absorption change and the spectral change of pulses by the modulation effects. Thus, to let us discriminate the modulation effects more clearly, a transparent sample CS_2 in a 1-mm cell was measured. The left-hand side of Fig. 11 shows both DTS's and DPS's. The experimental conditions were the same as for the

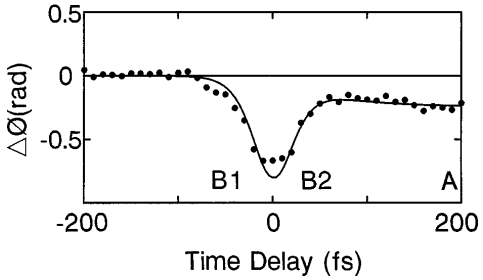

Fig. 12. Delay-time dependence of $\Delta\Phi$ (dots) for CS_2, derived from the FT of the interference data, and the fitting function (solid curve) given by Eq. (20). Conditions B1, B2, and A are satisfied at −50-, 50-, and 190-fs time delays, respectively (see Section 4).

R63 filter, except the excitation density is ~1.9 mJ/cm^2. Figure 12 shows the delay-time dependence of the average phase change in the probed region.[37] Since the femtosecond pump pulse has a broad bandwidth, Raman frequencies within the bandwidth are resonantly excited to cause an inertial nuclear motion of CS_2, which is time resolved in Fig. 12 as a delayed rise of $\Delta\Phi$. On the other hand, the instantaneous response that follows the pump-pulse profile at zero delay is due to the nonresonant electronic response.

The negative phase change is due to the positive nonlinear refractive index (n_2) in CS_2. Because of the nonresonant observation region, in Fig. 11 there is no net transmittance change; i.e., the spectrally integrated probe intensity is unchanged with and without excitation for all delays within experimental error. The spectral dependence of the DTS and the DPS is attributed to spectral changes of the probe pulse as a result of IPM, because the results on the left of Fig. 11 can be reproduced by the numerical simulation with only the time-dependent phase change assumed as follows.

First, to yield the response function, the time evolution in Fig. 12 was fitted to a phenomenological expression of the femtosecond optical Kerr dynamics[38–41] in CS_2:

$$\Delta\phi(t) = \alpha I_{\mathrm{ex}}(t) + \beta\theta(t)\exp(-t/\tau_d)[1 - \exp(-t/\tau_r)]. \quad (20)$$

The first term on the right represents the instantaneous electronic response, where $I_{\mathrm{ex}}(t)$ is the normalized pump-pulse intensity. The pulse fields are assumed to be FT-limited hyperbolic-secant fields as in Eq. (C7) below. The second term represents the nuclear orientational response with decay and rise times of τ_d and τ_r, respectively, and α and β are appropriate constants. Although the nuclear response consists of several origins with different kinetics, it is enough to consider only the orientational term for fitting the behavior until a 200-fs time delay.

We substitute $\tau_d = 1.6$ ps and $\tau_r = 75$ fs from the literature,[39,41] $\tau_{\mathrm{pr}} = \tau_{\mathrm{ex}} = 50$ fs, $\alpha/\beta = 1/0.36$, and -0.8 rad for the peak phase change. The solid curve in Fig. 12 is the fitting function $\Delta\phi(\tau)$. Near zero delay $\Delta\phi(\tau)$ shows a sharper peak than the experimental plot $\Delta\Phi(\tau)$ because $\Delta\Phi(\tau)$ is expressed as the convolution between $\Delta\phi(t)$ and the probe intensity $|E_{\mathrm{pr}}'(t)|^2$, as indicated in Eq. (B7) below.

Next, with the fitted response function $\Delta\phi(t)$, the following numerical calculations are performed[34]:

$$\begin{aligned} E_{\mathrm{pr}}(t) &= E_1(t)\exp(i\omega_{\mathrm{pr}}t), \\ E_{\mathrm{pr}}(t,\tau) &= E_1(t)\exp[i\omega_{\mathrm{pr}}t + i\Delta\phi(t+\tau)], \\ F[E_{\mathrm{pr}}(t)] &= R(\omega)\exp[i\Phi(\omega)], \\ F[E_{\mathrm{pr}}(t,\tau)] &= R(\omega,\tau)\exp[i\Phi(\omega,\tau)], \\ \Delta T/T(\omega,\tau) &= [R^2(\omega,\tau) - R^2(\omega)]/R^2(\omega), \\ \Delta\Phi(\omega,\tau) &= \Phi(\omega,\tau) - \Phi(\omega). \end{aligned} \quad (21)$$

The results are shown on the right-hand side of Fig. 11. Note that the calculations above are reduced to the level population term in the perturbation limit as discussed in Ref. 34. The calculated results on the right reproduce the characteristic features of the experimental results on the left. Since only the phase change is assumed here, it is verified that the observed dispersion relations are caused by the IPM of the probe pulse.

In Fig. 11 the DTS's show spectral shifts and broadening of the probe at ± 50 and 0 fs, respectively, and both DPS's and DTS's show transient oscillations at ± 120 fs. These signals can be explained from Fig. 12. At zero delay, for example, since the probe phase decreases at the leading edge and increases at the trailing edge, the probe spectrum shows both red and blue shifts, resulting in spectral broadening. This is analogous to self-phase modulation,[42,43] since the pump and the probe can be identified owing to their complete overlap at zero delay. In contrast, at 190 fs the spectra show little wavelength dependence; i.e., there is a flat spectrum in the DPS and no sizable signal in the DTS, as is expected for a nonresonant observation region. This is because the probe phase is not modulated appreciably at this delay, owing to an almost steady phase change as shown in Fig. 12. Note also that at 120 fs the DTS's show an increase toward longer wavelengths if the oscillations are eliminated by smoothing. This is because at this delay the probe experiences an increase in the refractive index that is due to the inertial nuclear motion, resulting in a slight red shift. This delayed nuclear motion is time resolved in Fig. 12.

Concerning the K–K relations, the results at -120 and -50 fs satisfy the relations qualitatively, while at -20 and 0 fs the results show a qualitative difference from the K–K relations. In particular, at 0 fs both the DTS and the DPS are even functions with respect to the probe center frequency. This is unusual, because the K–K inversion transforms even functions into odd functions. Further, the signals at 50 fs seem to satisfy the K–K relations with reversed signs, because the DPS has the same sign as that at -50 fs, and the DTS has the sign opposite that at -50 fs at corresponding wavelengths. So do the signals at 120 fs, where the relative phase of the oscillations between the DTS and the DPS is shifted by π from that at -120 fs. At 190 fs both the DTS and the DPS are almost constant, so that the K–K relations are not violated. In summary, the signals for CS_2 show unusual dispersion relations, depending on the time delay, in marked contrast to those for the R63 filter, exhibiting the ordinary K–K relations qualitatively. This will be discussed in detail in Section 4.

C. Transient Oscillations

We have observed transient oscillations in the DTS and the DPS for both the R63 filter and CS_2. Transient oscillations in the DTS are reported by many authors[26–30] and are considered to be caused by the following mechanism. The transient grating is formed by the coupling of a pump field and a probe-induced polarization to diffract the pump partially in the direction of the probe. The interference between the probe and the diffracted pump causes the spectral oscillations. The phenomenon is called perturbed free-induction decay[29] (PFID). When the probe pulse is short enough to be well approximated by a δ function, the oscillations that are due to PFID appear only at negative delays until the phase relaxation time. In fact, in the previous reports[26–30] the oscillations were observed only at negative delays, because the previous experiments were performed for resonant materials with probe pulses much shorter than the phase relaxation time.

There is, however, another mechanism that will allow the oscillations,[34] which are produced by the level-population term, to appear with the same amplitude for both negative and positive delays, as in the present study. This can be readily understood by use of the FT as follows.[34] When $1 \gg \Delta k \gg \Delta n$, the probe field is

$$\begin{aligned} &E(t)\exp[i\omega_0 t - \Delta k(t+\tau)\omega_0 L/c] \\ &\quad \sim [E(t) - \delta E(t+\tau)]\exp(i\omega_0 t) \\ &\quad \xrightarrow{\text{FT}} E(\omega-\omega_0)\{1 - \delta\exp[i(\omega-\omega_0)\tau]\}, \\ &\Delta T/T(\omega,\tau) \sim -2\delta\cos(\omega-\omega_0)\tau, \\ &\Delta\Phi(\omega,\tau) \sim -\delta\sin(\omega-\omega_0)\tau. \end{aligned} \tag{22}$$

When $1 \gg \Delta n \gg \Delta k$,

$$\begin{aligned} &E(t)\exp[i\omega_0 t - i\Delta n(t+\tau)\omega_0 L/c] \\ &\quad \sim [E(t) - i\delta E(t+\tau)]\exp(i\omega_0 t) \\ &\quad \xrightarrow{\text{FT}} E(\omega-\omega_0)\{1 - i\delta\exp[i(\omega-\omega_0)\tau]\}, \\ &\Delta T/T(\omega,\tau) \sim 2\delta\sin(\omega-\omega_0)\tau, \\ &\Delta\Phi(\omega,\tau) \sim -\delta\cos(\omega-\omega_0)\tau. \end{aligned} \tag{23}$$

Here $\delta \ll 1$, and the response of $\Delta n(t)$ and $\Delta k(t)$ is assumed to follow the pump intensity profile $I(t)$. Owing to the $\exp[i(\omega-\omega_0)\tau]$ terms, a net phase change of the probe is accompanied by a spectral shift in the DTS, whereas a net amplitude change is accompanied by a spectral shift in the DPS. Since the electronic response term follows the pump-pulse profile instantaneously, the signals for CS_2 are approximately expressed by Eqs. (23), except near zero delay, where the Taylor expansion to first order is insufficient, as is demonstrated below with Eq. (33). Physically the modulations of the probe phase and the amplitude, IPM and IAM cause the oscillations that appear for both negative and positive time delays within the probe-pulse duration. If the phase relaxation time is much shorter than the probe pulse, then the PFID term also gives the same amplitude of oscillations for both negative and positive delays, although the oscillations by PFID are different in mechanism from those by IPM and IAM.

4. KRAMERS–KRONIG RELATIONS IN TIME-RESOLVED SPECTROSCOPY

The K–K relations[1,2] connect the real and the imaginary parts of the linear susceptibility $\chi(\omega)$. For the nonlinear susceptibility $\chi^{(n)}(\omega_1,\ldots,\omega_n)$, with tunable monochromatic light sources there also exist dispersion relations similar to the K–K relations as long as the causality condition is satisfied for a response function.[3–6] On the other hand, in time-resolved spectroscopy with pulsed light sources the standard K–K relations are not valid, because the pump pulse induces the time-dependent change in the state of a material even before the probe field is applied, resulting in the causality condition's being broken between the probe field and the probe-induced polarization.[8] Since the DPS and the DTS are proportional to the change in the real and the imaginary parts of the susceptibility, respectively, the experimental results here are good samples to be compared directly with the K–K relations. The dispersion relations for both experimental and calculated results show a larger discrepancy from the K–K relations for CS_2 than for the CdS_xSe_{1-x}-doped glass. This result is explained by the theoretical treatment of time-resolved dispersion relations along the line of the previous publication,[8] and useful practical criteria for applying the K–K relations to time-resolved data are deduced.

A. Numerical Simulations

To study characteristics of time-resolved dispersion relations, we have performed the numerical simulations from Eqs. (16) and (17) in the following three cases:

1. $T_2 < \tau_{pr} = \tau_{ex} < T_1$,
2. $\tau_{pr} = \tau_{ex} > T_2 > T_1$,
3. $\tau_{pr} = T_1 < T_2 < \tau_{ex}$.

The first case is already calculated in Figs. 9(a) and 10 for simulating the results for the R63 filter and may be most frequently encountered experimentally among the three cases. In this case the probe-pulse duration is comparable with the rise time of $N^{(2)}(t)$, whereas it is much shorter than the decay time, so that the distortion of $\chi^{(3)}(\omega,\tau)$ from $\chi^{(1)}(\omega)$ is significant at zero delay but not at 100 fs.

The second case is shown in Figs. 9(b) and 13 for the conditions

$$T_1 = 15\text{ fs}, \qquad T_2 = 30\text{ fs}, \qquad \tau_{pr} = \tau_{ex} = 60\text{ fs},$$

$$\Lambda = \lambda_{pr} = \lambda_{ex} = 620\text{ nm}.$$

In this case the distortion is significant for all $\chi^{(3)}(\omega,\tau)$'s,

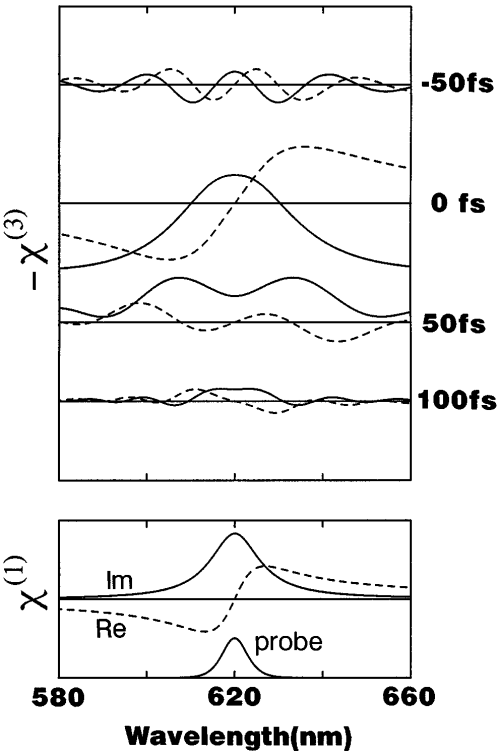

Fig. 13. $\chi^{(3)}(\omega,\tau)$ calculated from Eq. (17) for the condition $\tau_{pr} = \tau_{ex} > T_2 > T_1$ ($T_1 = 15$ fs, $T_2 = 30$ fs, $\tau_{pr} = \tau_{ex} = 60$ fs, and $\Lambda = \lambda_{pr} = \lambda_{ex} = 620$ nm). The assumed temporal dynamics is displayed in Fig. 9(b). $-2\,\mathrm{Im}\,\chi^{(3)}$ and $-\mathrm{Re}\,\chi^{(3)}$ correspond to DTS's and DPS's, respectively. Upper part, Real (dashed curves) and imaginary (solid curves) parts of $\chi^{(3)}(\omega)$. Lower part, $\chi^{(1)}(\omega)$ and the probe spectrum.

where the distortion is caused by IAM because of the exact resonance. At −50 and 100 fs it seems that the K–K relations and the K–K relations with reversed signs, respectively, hold. This is analogous to the signals for CS_2 at ±50 fs in Fig. 11. Clearly known from $\chi^{(3)}(\omega, \tau)$ at 100 fs, in this example the modulation effect gives a larger contribution to the signal than the intrinsic spectral change, $\chi^{(1)}(\omega)$, in the system. This is because $N^{(2)}(t)$ changes as rapidly as $E_{\mathrm{pr}}(t)$ and because T_2 is shorter than τ_{pr} such that $\chi^{(1)}(\omega)$ has a weak wavelength dependence in the probed spectral region.

The third case is shown in Figs. 9(c) and 14 for conditions that are the same as in the second case, except that $\tau_{\mathrm{pr}} = 15$ fs. In Fig. 14 no oscillations appear, because the probe pulse is short enough to be insensitive to the modulation effect. (As mentioned in Subsection 3.C, even for this condition the PFID term still gives significant oscillations for negative delays as long as $-T_2$.) Since $\chi^{(3)}(\omega, \tau)$ is almost proportional to $\chi^{(1)}(\omega)$ throughout the delays, the K–K relations hold approximately for all $\chi^{(3)}(\omega, \tau)$.

From Figs. 9, 10, 13, and 14 we can expect the following criteria for the validity of the K–K relations in time-resolved spectroscopy: The distortion from the K–K relations becomes significant when the probe pulse undergoes a rapid change within the pulse duration to suffer induced modulation effects. If the probe pulse is much shorter than the pump pulse, as in the third case, or if the delay time is much longer than the probe-pulse duration, as in the first case, then the K–K relations hold approximately. This prediction is analytically treated in the following subsections.

B. Theoretical Consideration

The K–K relations are based on causality; i.e., there is no polarization induced before an external field is applied. The relations are derived from the complex integration of $\chi(\omega)/(\omega - \omega_0)$ in the lower half of the complex ω plane, where $\chi(\omega)$ has no singularities as a consequence of the causality condition.[1,2]

The polarization $P(t)$ induced in a material by a probe pulse field $E(t)$ is expressed as

$$P(t) = \chi(t) \otimes E(t) = \int_0^\infty \mathrm{d}t' \chi(t') E(t - t'), \qquad (24)$$

where ⊗ denotes the convolution operation, $\chi(t)$ is a polarization response function that is zero for $t < 0$ by the causality condition, and time zero is marked at the probe-pulse peak. [$\chi(t)$ corresponds to $f_2(t)$ in Eqs. (C5) below.] The linear susceptibility function is given by the FT of Eq. (24) as

$$\chi(\omega) = F[P(t)]/E(\omega) = \int_0^\infty \mathrm{d}t \, \exp(-i\omega t)\chi(t). \qquad (25)$$

The function $\chi(\omega)$ satisfies the K–K relations because it has no poles in the lower ω half-plane, as is readily deduced from $t > 0$ in $\exp(-i\omega t)$. In time-resolved spectroscopy, however, the causality condition is not satisfied between the incident probe field and the induced polarization because a pump pulse is applied to cause the following polarization change:

$$\Delta P(t) = \chi(t) \otimes [E(t)\Delta N(t)] = \int_0^\infty \mathrm{d}t' \chi(t') E(t - t') \Delta N(t - t'), \qquad (26)$$

where $\Delta N(t)$ represents the change in the level-population difference that is due to the pump and depends on τ such that $\Delta N(t) = \Delta N'(t + \tau)$. [$\Delta N(t)$ corresponds to $N^{(2)}(t)$ in Eq. (C2) below but is not necessarily limited to second order here.] Equation (26) describes the level-population term for a two-level system. The coherent coupling term is discussed in Subsection 4.F. From Eq. (26), the susceptibility change is expressed by

$$\Delta\chi(\omega) = F[\Delta P(t)]/E(\omega) = \chi(\omega) \int_{-\infty}^{\infty} \mathrm{d}t \, \exp(-i\omega t) E(t) \Delta N(t)/E(\omega). \qquad (27)$$

In general $\Delta\chi(\omega)$ has poles in both half-planes because the integration is over all t in Eq. (27). Therefore the K–K relations are not generally satisfied. However, the K–K relations are strictly satisfied in the following three special cases:

A. $\Delta N(t)$ is steady or $E(t)$ is a δ function.
B. $\Delta N(t)$ is zero over $t < 0$ (negative delays).
C. $E(t) = 0$ over $t < 0$.

In the following subsections these conditions are closely examined. When we claim below that the K–K relations are applicable, it is assumed that the DTS's (or the DPS's) are known in the whole frequency range, because theoretically the tail of the probe-pulse spectrum has a finite amplitude for any large frequency. Experimentally this is the ideal case in which the signal-to-noise ratio is infinite.

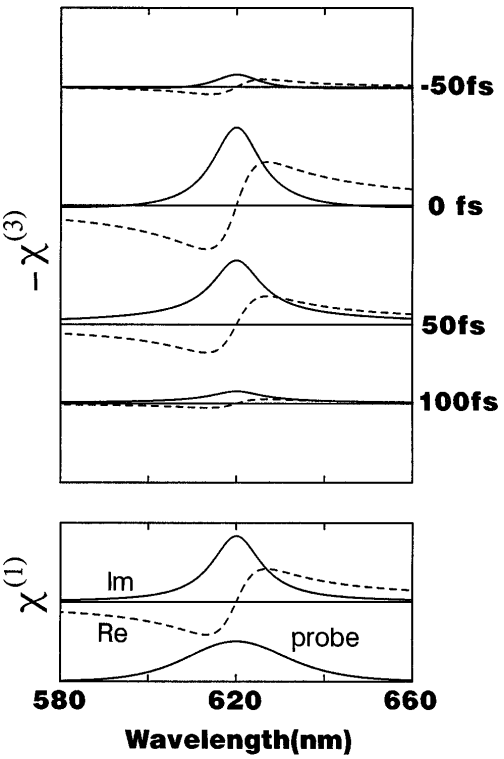

Fig. 14. $\chi^{(3)}(\omega, \tau)$ calculated from Eq. (17) for the condition $\tau_{\mathrm{pr}} = T_1 < T_2 < \tau_{\mathrm{ex}}$ ($T_1 = 15$ fs, $T_2 = 30$ fs, $\tau_{\mathrm{pr}} = 15$ fs, $\tau_{\mathrm{ex}} = 60$ fs, and $\Lambda = \lambda_{\mathrm{pr}} = \lambda_{\mathrm{ex}} = 620$ nm). The assumed temporal dynamics is displayed in Fig. 9(c). Upper part, Real (dashed curves) and imaginary (solid curves) parts of $\chi^{(3)}(\omega, \tau)$. Lower part, $\chi^{(1)}(\omega)$ and the probe spectrum.

C. Steady-State Condition

If condition A is satisfied, the K–K relations hold as follows:

A1. When $\Delta N(t)$ is constant (ΔN_0),

$$\Delta\chi(\omega) = \frac{\chi(\omega)}{E(\omega)} \int_{-\infty}^{\infty} \mathrm{d}t \, \exp(-i\omega t) E(t) \Delta N_0 = \Delta N_0 \chi(\omega). \tag{28}$$

A2. When $E(t)$ is a δ function [$E_0\delta(t)$],

$$\Delta\chi(\omega) = \frac{\chi(\omega)}{E_0} \int_{-\infty}^{\infty} \mathrm{d}t \, \exp(-i\omega t) E_0 \delta(t) \Delta N(t)$$

$$= \Delta N(0)\chi(\omega) = \Delta N'(\tau)\chi(\omega) \tag{29}$$

(Ref. 35). Note that conditions A1 and A2 are physically equivalent because both can be described as follows: $\Delta N(t)$ is steady during the probe-pulse duration. Therefore we can call them both the steady-state condition. Under the steady-state condition the K–K relations are satisfied because the probe pulse is not subject to the induced modulation effects, and the wavelength dependence of $\Delta\chi(\omega)$ is caused only by an intrinsic susceptibility change in the material. Why the K–K relations hold approximately at 100 fs in Fig. 10 and at all delays in Fig. 14 is explained by the steady-state condition.

Let us examine whether the steady-state condition is satisfied for the experimental results in Figs. 6 and 11 by using the delay-time dependence $\Delta\Phi(\tau)$ in Figs. 7 and 12, which is approximately proportional to $\Delta\phi(t)$ or $\Delta N(t)$. For the R63 filter, $\Delta\Phi(\tau)$ is nearly steady at 100 and 180 fs within the probe-pulse duration in Fig. 7, to satisfy the condition. In Fig. 6, therefore, the K–K relations hold approximately at 100 and 180 fs. For CS_2, at 190 fs the DTS shows zero signal and the DPS shows a flat spectrum. These signals can be explained self-consistently as follows: At 190 fs the condition is satisfied because $\Delta\Phi(\tau)$ is nearly steady, as seen in Fig. 12. Then, from Eq. (28), $\Delta\chi(\omega)$ should be proportional to $\chi(\omega)$. Further, from the large detuning condition it is expected that Im $\chi(\omega)$ will be zero and that Re $\chi(\omega)$ will be constant. Consequently, Im $\Delta\chi(\omega)$ ($\propto$DTS) is zero and Re $\Delta\chi(\omega)$ ($\propto$DPS) is constant, as was observed.

Here the K–K relations are discussed only for the probed spectral region, but if the measurement is performed in the whole frequency range with an ideal δ-function probe pulse, Re $\Delta\chi(\omega)$ near 620 nm should be related through the K–K relations to Im $\Delta\chi(\omega)$ far from 620 nm. For example, the DPS that is due to the nuclear response at 120 and 190 fs in Fig. 11 should be related to the DTS, which is caused by excitation of all the Raman modes within the pump bandwidth. There are several studies of low-frequency dispersion relations of Re $\chi^{(3)}$ and Im $\chi^{(3)}$ by the Raman-induced Kerr effect, such as the FT four-wave mixing method.[44] In such methods femtosecond optical-heterodyne-detected optical-Kerr-effect signal intensity as a function of time delay is Fourier transformed to yield the low-frequency dispersion as a function of $\Delta\omega$, where $\Delta\omega$ is a difference frequency within the pump bandwidth, giving information essentially equivalent to frequency-domain dynamic light-scattering data.[45] However, the present measurement is distinctive in that the high-frequency (visible-frequency) dispersion as a function of the probe frequency is obtained, which is a Fourier transform of probe-induced polarization decay as a function of time. Hence dispersion relations that are due to the nonresonant electronic response can be directly measured as shown at -20 and 0 fs in Fig. 11 although the true dispersion is distorted by the IPM effect, owing to the lack of time resolution of the pulse. The true dispersion is distorted by the IPM effect. The difference from the conventional Kerr measurements is clearly described in Appendix D.

D. Kramers–Kronig Relations with Reversed Signs

Condition A is a basic criterion for applying the K–K relations under which the induced modulation effects are avoided. On the other hand, conditions B and C are rather special ones, under which the modulated spectra of the probe pulse also satisfy the K–K relations. For condition B there are two cases, as follows:

B1. When $\Delta N(t)$ is zero over $t < 0$ (negative delays), then

$$\Delta\chi(\omega) = \frac{\chi(\omega)}{E(\omega)} \int_{0}^{\infty} \mathrm{d}t \, \exp(-i\omega t) E(t) \Delta N(t). \tag{30}$$

This function has no poles in the lower ω half-plane, so that it obeys the K–K relations.

B2. When $\Delta N(t)$ is zero for $t > 0$ (positive delays) and $\chi(\omega)$ is constant (χ_0), then

$$\Delta\chi(\omega) = \frac{\chi_0}{E(\omega)} \int_{-\infty}^{0} \mathrm{d}t \, \exp(-i\omega t) E(t) \Delta N(t). \tag{31}$$

Since this function has no poles in the upper ω half-plane, it obeys the K–K relations with reversed signs.

In order that $\chi(\omega) = \chi_0$, the rapid dephasing or large detuning condition must be satisfied.[34] Note that, with condition A1, it is enough that $\Delta N(t) = \Delta N_0$(constant) for $t < 0$ and $t > 0$ in the above two conditions.

For B1 and B2 additional conditions are required because $1/E(\omega)$ may generally cause singularity. First, $E(\omega)$ should be a real function, because otherwise the relation between the real and the imaginary parts of $1/E(\omega)$, which has nothing to do with the K–K relations, is reflected in $\Delta\chi(\omega)$. Second, $1/E(\omega)$ must not have poles for $|\omega| < \infty$ in the lower and the upper half-planes for B1 and B2, respectively. Third, $\Delta\chi(\omega)/(\omega - \omega_0)$ should fall off more rapidly than $1/\omega$. Since $\Delta\chi(\omega)$ can be rewritten in the form

$$\Delta\chi(\omega) = \chi(\omega) \int \mathrm{d}\omega' \Delta N(\omega') E(\omega - \omega')/E(\omega), \tag{32}$$

it is necessary that $E(\omega - \omega')/E(\omega) \to \mathrm{O}(\omega^{\delta})$, with $\delta \leqq 0$ as $\omega \to \infty$. These conditions are satisfied for, e.g., a hyperbolic-secant or Lorentzian envelope $E(\omega)$ but not for a Gaussian envelope $E(\omega)$. Since the envelope of a mode-locked laser pulse is well approximated by a hyperbolic-secant function,[46] the additional conditions can be satisfied. Note that the additional conditions are not sufficient but are only necessary conditions.[47]

For the R63 filter, at negative delays the K–K relations hold qualitatively because $\Delta\Phi(\tau)$ rises at the trailing edge of the probe pulse to satisfy condition B1, whereas near zero delay the relations do not hold, because none of the conditions are satisfied owing to the rapid increase of $\Delta\Phi(\tau)$ over the whole probe-pulse duration. In Fig. 10 $\chi^{(3)}(\omega, \tau)$ at zero delay is distorted by the induced modulation effects to show dispersion relations substantially different from $\chi^{(1)}(\omega)$, but qualitative features of the dispersion relations are still consistent with the K–K relations, because the wavelength dependence of $\chi^{(1)}(\omega)$ dominates that of $\chi^{(3)}(\omega, \tau)$ in Eq. (18).

For CS_2, at −50 fs condition B1 is approximately satisfied because $\Delta\Phi(\tau)$ rises at the trailing edge of the pulse, whereas at 50 fs condition B2 is approximately satisfied because $\Delta\Phi(\tau)$ decays to a constant at the leading edge and $\chi(\omega)$ has negligible wavelength dependence. Therefore the standard and the sign-reversed K–K relations hold approximately at −50 and 50 fs, respectively. As mentioned in Subsection 3.C, these signals can also be explained qualitatively by relations (23), where the real part (cos $\omega\tau$) and the imaginary part (sin $\omega\tau$) of $\exp(i\omega\tau)$ are strictly related to each other through the K–K relations but the signs of the relations depend on τ. For IPM spectra the DPS cannot be reproduced from only the DTS by the K–K relations; additional information, the sign of τ or the time derivative of the phase change, is required. It is considered that the sign reversal of the K–K relations is peculiar to time-resolved spectroscopy, where the change can occur as a result of the pump even before the probe field is applied.

To fulfill condition B2, $\chi(\omega)$ must be constant. This is so only when the phase relaxation time is much shorter than the pulse duration (rapid dephasing) or the detuning is much larger than the pulse spectral width (large detuning) as in the case of CS_2. Because of this restriction the sign-reversed relations are usually not observed for resonant materials. For example, the signals for CdS_xSe_{1-x}-doped glass qualitatively show not the sign-reversed relations but the standard K–K relations, even for positive delays. Although the numerical simulation exhibits the sign-reversed relations at 50 and 100 fs in Fig. 13, extreme conditions are imposed there, such as $T_1 = 15$ fs and $T_2 = 30$ fs; i.e., dephasing is due only to energy relaxation.

On the other hand, condition B1 has no such restriction. Therefore it can be agreed that in time-resolved spectroscopy the ordinary K–K relations are approximately applicable for negative time delays. This result is important because an optical Stark effect in time-resolved spectroscopy, which is caused by the PFID term in the third-order approximation, appears from negative to zero delay.[29,30] Condition B1 assures us that the K–K relations can be applied to optical-Stark-effect signals for negative delays to yield the refractive-index change in the spectral range of absorption.

For CS_2, at zero delay both real and imaginary parts are even functions with respect to the probe center frequency, that is, substantially different from the standard K–K relations because none of the conditions is satisfied. Since the signal at zero delay is caused mainly by the instantaneous electronic response implied in Eq. (20), we have performed the simulation, Eqs. (21), assuming $\Delta\phi(t) = \alpha I_{ex}(t)$, to obtain the result shown at the top of Fig. 15. Here, both the DTS and the DPS are even functions, from the time symmetry of $\Delta\phi(t)$, whereas the zero-delay signal in Fig. 11 shows a slight asymmetry that is due to the contribution of the nuclear response term in Eq. (20).

The calculated equation for the top plot of Fig. 15 can be expanded as follows:

$$E(t)\exp[i\Delta\phi(t)] = E(t)[1 + i\Delta\phi(t) - (1/2)\Delta\phi^2(t) - (i/6)\Delta\phi^3(t) + \ldots]. \quad (33)$$

Since $\Delta\phi(t)$ is an even function with respect to time zero, the FT of Eq. (33) is an even function with respect to zero frequency. In the lowest order the spectral broadening observed in the DTS is caused by the third term on the right-hand side, $-(1/2)\Delta\phi^2(t)$ (fifth-order nonlinearity), whereas the broadening in the DPS is caused by the second term $i\Delta\phi(t)$ (third-order nonlinearity). Note that the $(4m + 1)$th order of nonlinearity is purely imaginary and that the $(4m - 1)$th order is purely real.

The result in the top plot of Fig. 15 can be divided into two parts, one originating from $\Delta\phi_-(t)$ for $t < 0$ (left) and the other from $\Delta\phi_+(t)$ for $t > 0$ (right), as shown

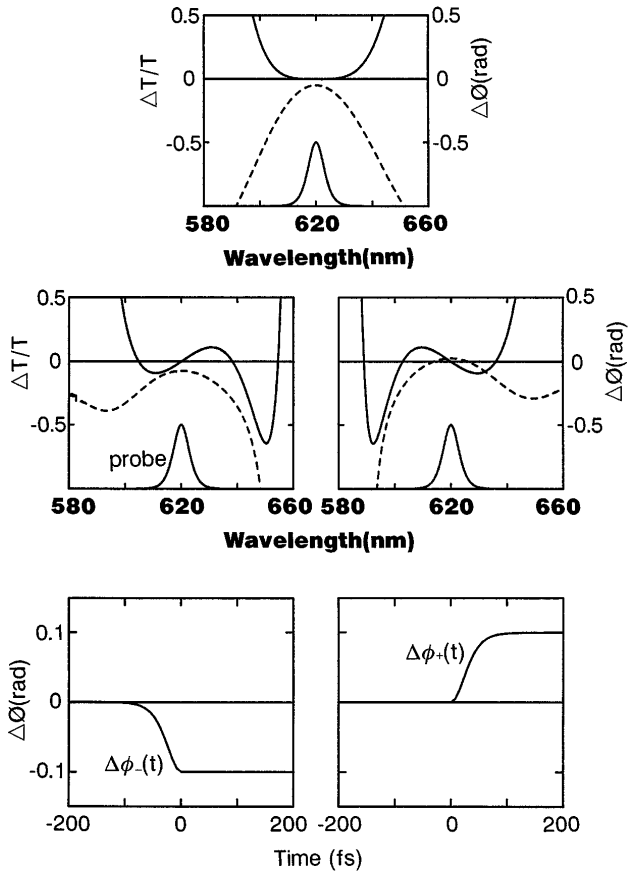

Fig. 15. Top, DTS (solid curves) and DPS (dashed curves) at zero delay calculated from Eqs. (21) with the phase change $\Delta\phi(t) = \alpha I_{ex}(t)$. Middle, DTS (solid curves) and DPS (dashed curves) calculated with $\Delta\phi_\pm(t)$, shown in the bottom plots. The sum of both middle plots gives the top plot. Bottom, Time evolution of the phase change $\Delta\phi_\pm(t)$, which satisfies $\Delta\phi_-(t) + \Delta\phi_+(t) = \Delta\phi(t)$. Left, $\Delta\phi_-(t) = \alpha I_{ex}(t)$ for $t < 0$, $\Delta\phi_-(t) = \alpha I_{ex}(0)$ for $t > 0$. Right, $\Delta\phi_+(t) = 0$ for $t < 0$, $\Delta\phi_+(t) = \alpha I_{ex}(t) - \alpha I_{ex}(0)$ for $t > 0$.

in the bottom plots of Fig. 15. The left-hand plot satisfies condition B1 for the standard K–K relations, and the right-hand plot satisfies condition B2 for the sign-reversed K–K relations.[47] Their sum, on the other hand, never satisfies the K–K relations, because complex integration cannot be performed in either half-plane without leaving residues.

E. Non-Transform-Limited Case

When non-transform-limited pulses are used for the probe, i.e., when $E(\omega)$ is a complex function, the K–K relations generally do not hold, except for condition A1, because the relation between the real and the imaginary parts of the pulse field, which has nothing to do with the causality principle, is reflected in the signals.[48–50] However, there is a special case in which the K–K relations hold even for non-transform-limited pulses, as follows:

C. $E(t) = 0$ for $t < 0$, such as a single-sided exponential.

This is rephrased as

C. The real and the imaginary parts of $E(\omega)$ are related through the K–K relations.

In this case the K–K relations apply to $\Delta\chi(\omega)$ for any time delay. When $E(t) = 0$ for $t > 0$ and $\chi(\omega) = \chi_0$, the relations with reversed signs apply as in the case of condition B. Note that displacing $E(t)$ from the time origin does not lead to condition C's being satisfied, because this displacement is equivalent to a change of time delay, i.e., the multiplication by a factor of $\exp(i\omega\tau)$ as in Eq. (19).

If condition C is satisfied, the K–K relations hold even at zero delay for CS_2. Figure 16 is the simulation at zero delay, where it is assumed that the probe has a single-sided-exponential envelope $E(t)$ with a 30-fs FWHM intensity and $\Delta\phi(t)$ is the same as in Fig. 15. In Fig. 16 the K–K relations hold rigorously, because both the DTS and the DPS are limited by a finite value to satisfy $\Delta\chi(\omega) \to 0(\omega^{\delta})$ with $\delta \leqq 0$ as $|\omega| \to \infty$. This is proved in Appendix E.

F. Weak-Probe Condition

Only the level-population term [Eq. (26)] has been considered in the deduction of conditions A–C, but a similar argument can apply to the coherent coupling terms, as follows. The coherent coupling term, to second order in the pump field and to first order in the probe field, is, for example, expressed as

$$\Delta P_c(t) = \chi(t) \otimes [E_{\mathrm{ex}}(t)\Delta N_c(t)],$$

$$\Delta N_c(t) = \eta(t) \otimes [E_{\mathrm{ex}}{}^{*}(t)P(t)]$$

$$= \int_{-\infty}^{t} \mathrm{d}t'\eta(t - t')[E_{\mathrm{ex}}{}^{*}(t')P(t')], \qquad (34)$$

where the asterisk denotes the complex conjugate, $E_{\mathrm{ex}}(t)$ is a pump-pulse field, and $\eta(t)$ is a population-response function that is zero for $t < 0$ [corresponding to $f_1(t)$ in Eqs. (C5)]. This is the PFID term, which has already been mentioned frequently in this paper. For condition A, if $E(t) = E_0\delta(t)$, $P(t) = E_0\chi(t)$, from Eq. (24). Then it can readily be shown that $\Delta P_c(t) = 0$ for $t < 0$. Therefore condition A holds for this term also. For condition B, if $E_{\mathrm{ex}}(t) = 0$ for $t < 0$ and $t > 0$, the Fourier integration can be over $t > 0$ and $t < 0$, respectively. Further, the susceptibility change is expressed by

$$\Delta\chi_c(\omega) = \chi(\omega) \int \mathrm{d}\omega' E_{\mathrm{ex}}(\omega')\Delta N_c(\omega - \omega')/E(\omega)$$

$$= \chi(\omega) \int \mathrm{d}\omega' E_{\mathrm{ex}}(\omega')\eta(\omega - \omega') \int \mathrm{d}\omega'' E_{\mathrm{ex}}{}^{*}(\omega'')$$

$$\times \chi(\omega - \omega' - \omega'')E(\omega - \omega' - \omega'')/E(\omega), \qquad (35)$$

which requires the same additional conditions for $E(\omega)$. Therefore condition B also holds. Even for the higher order in the pump field, one can readily see that a similar argument can be made insofar as the probe field is weak enough to be limited to first order.

In summary, conditions A and B are criteria that are valid for time-resolved signals with any order of nonlinearity in the weak-probe-field limit. To satisfy either of conditions A and B, it is necessary that the probe field be weak enough not to cause nonlinear change by the probe itself. (Condition C is the exception for which the weak-probe condition is not necessary, as is discussed in Appendix E.) From this viewpoint the signals at zero delay for CS_2 do not satisfy the weak-probe condition, because the pump can be identified with the probe, owing to the complete overlap of the pump and the probe, so that the polarization change is expressed not by the first order in the probe field but, effectively, by a higher order.

G. Relation with Steady-State Nonlinear Spectroscopy

In this subsection we discuss the relation between time-resolved spectroscopy and nonlinear spectroscopy with tunable monochromatic light.

If we assume the long-pump-pulse limit, in which

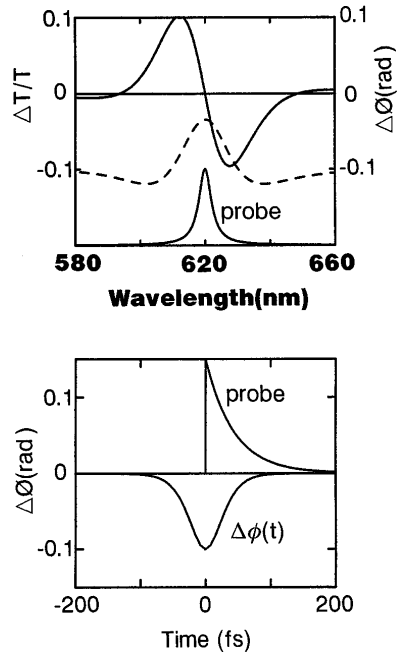

Fig. 16. Upper plot, DTS and DPS (dashed curve) at zero delay and the probe spectrum, calculated for condition C. Lower plot, Temporal dynamics used for calculating the upper plot. The probe-pulse shape is a single-sided exponential, and the phase change is $\Delta\phi(t) = \alpha I_{\mathrm{ex}}(t)$, which is the same as that used in Fig. 15.

steady-state condition A1 is satisfied, we obtain the nonlinear susceptibility with tunable monochromatic light; for a steady monochromatic pump, Eq. (17) becomes

$$\chi^{(3)}(\omega) = 2\mu N_0 \frac{\mu^3}{\hbar^3} \frac{i}{2} \frac{1}{i(\omega - \Omega) + 1/T_2} \frac{T_1}{T_2} \times \frac{1}{(\omega_{ex} - \Omega)^2 + (1/T_2)^2} E^2 . \quad (36)$$

We obtain this function by tuning a probe light over the whole frequency, and it strictly obeys the K–K relations. However, if the probe is also used for the pump, to cause saturation by the probe itself, Eq. (36) is written as

$$\chi^{(3)}(\omega) = \frac{N_0\mu^2}{\hbar} i \frac{1}{i(\omega - \Omega) + 1/T_2} \frac{T_1}{T_2} \frac{1}{(\omega - \Omega)^2 + (1/T_2)^2} \times \left(\frac{\mu}{\hbar} E\right)^2 . \quad (37)$$

This function has poles in both the upper and the lower half-planes, so that spectra for self-saturation by the probe itself do not obey the K–K relations.[2] Equation (37) is the perturbation limit of

$$\chi_s(\omega) - \chi^{(1)}(\omega) = \frac{N_0\mu^2}{\hbar} \left[\frac{\Omega - \omega - i/T_2}{(\Omega - \omega)^2 + (1/T_2)^2 + |u|^2 T_1/T_2} - \frac{\Omega - \omega - i/T_2}{(\Omega - \omega)^2 + (1/T_2)^2} \right], \quad (38)$$

where u is the pump Rabi frequency given by $u = \mu E/\hbar$. The first term $\chi_s(\omega)$ is the steady-state solution[2] of the optical Bloch equations. This term can be rewritten as

$$\chi_s(\omega) = \frac{\mu^2}{\hbar} N_s(\omega) \frac{\Omega - \omega - i/T_2}{(\Omega - \omega)^2 + (1/T_2)^2} , \quad (39)$$

where $N_s(\omega)$ is expressed as

$$N_s(\omega) = N_0 \frac{(\Omega - \omega)^2 + (1/T_2)^2}{(\Omega - \omega)^2 + (1/T_2)^2 + |u|^2 T_1/T_2} . \quad (40)$$

This is the steady-state solution of the population difference without the perturbation approximation. If $N_s(\omega)$ is prepared by a monochromatic pump fixed at $\omega = \omega_{ex}$, then the real and the imaginary parts of Eq. (39) are rigorously related through the K–K relations because $N_s(\omega) = N_s(\omega_{ex}) =$ constant.[51] Since the steady-state solution $\chi_s(\omega)$ is derived without the perturbation approximation, the K–K relations hold for any large pump field E ($\propto u$) beyond the third-order perturbation regime if the nonlinear change is caused by a monochromatic pump and if the probe field is limited to first order.[4] Even with multicolored pump beams, if their frequencies are fixed while the probe frequency is scanned over the whole frequency the K–K relations are strictly satisfied. This is the criterion for the K–K relations to be applicable in nonlinear spectroscopy with tunable monochromatic light. Condition A in time-resolved spectroscopy is a natural extension of this criterion, since it can be expressed in the frequency domain as "the frequency range of the Fourier component of the nonlinear dynamics is much narrower than that of the probe," whereas conditions B and C are specific to time-resolved spectroscopy.

5. CONCLUSIONS

The breakdown of the K–K relations is caused by induced modulation effects. As is known from condition A2, for which distortion by modulation effects is absent, the modulation effects appear as long as a probe-pulse duration is finite. When a more rapid phenomenon than the time resolution is probed, the modulation effects become evident and mask the response function, which obeys the causality principle. In other words, the finite spectral width of the probe, which is responsible for the finite time resolution, prohibits the correct observation of the response function over the whole frequency range owing to modulation effects. To obtain dispersion relations that rigorously satisfy the K–K relations, a δ-function probe pulse must be used.

The time-resolved dispersion relations for nonresonant materials such as CS_2 are due only to the induced modulation effects, $F[E(t)\Delta N(t)]/E(\omega)$, which differ substantially from the standard K–K relations. For absorptive materials such as the R63 filter, on the other hand, the dispersion relations depend on both the intrinsic susceptibility change, $\chi(\omega)$, and the modulation effects, $F[E(t)\Delta N(t)]/E(\omega)$, so they are not much different from the standard K–K relations owing to the factor of $\chi(\omega)$. In general, near zero delay the modulation effects give significant distortion from the K–K relations owing to a rapid rise of the nonlinear change, whereas for longer delays the distortion is not significant, owing to slow relaxation of the nonlinear change.

The conditions for which the K–K relations are applicable in time-resolved spectroscopy are summarized as follows:

A. The nonlinear change is steady within the probe-pulse duration such that the modulation effects are absent. For example, the probe pulse is much shorter than the pump pulse, or the delay time is much longer than the probe-pulse duration.

B. In the case of transform-limited probe pulses, the probe-pulse peak arrives at the sample earlier than the nonlinear change occurs, i.e., at negative time delays.

C. In the case of non-transform-limited probe pulses, the real and the imaginary parts of the FT of the probe field are related through the K–K relations.

For condition A or B to be satisfied, it is necessary that the probe field be weak enough to be limited to first order in the nonlinear change.

The advantages of the FDI lie not only in its simple setup, stability, and simultaneous measurements of both the DTS and the DPS with a multichannel spectrometer but also in higher time resolution with a single measurement that uses the whole probe bandwidth simultaneously rather than with measurements that use one wavelength after another and spatial interference, where the bandwidth of the probe is reduced by wavelength selection. Even if spatial interference is detected through a multichannel spectrometer with $T = 0$, as is discussed with Eq. (13), it is difficult to obtain $\sin \Delta\Phi(\omega, \tau)$ depen-

dence for all ω. These advantages become more evident if femtosecond white-light continuum pulses are used.[49,50]

Femtosecond phase spectroscopy can solve the following problems, for example: First, because the DTS and the DPS carry mutually independent information that cannot be reproduced by the K–K relations, owing to the induced modulation effects, direct measurement of both the DTS and the DPS is necessary to extract the intrinsic spectral change from the modulated spectra. This problem is crucial when multilevel systems are studied.[52] Second, new aspects of femtosecond responses, especially those that are due to nonresonant excitation, can be illuminated, such as an optical Stark shift in excitonic states and optical Kerr dynamics in transparent Kerr media. The former is nothing but a net phase change in the resonant region in terms of phase spectroscopy, so that the shift can be better characterized by the DPS. For the latter the high-energy dispersion in the visible region can be studied by measurement of the DPS by use of continuum pulses, while by the conventional methods such as FT four-wave mixing[44] only the low-energy dispersion that is due to the nuclear response is obtained. Even though wavelength selection of the continuum is employed with the conventional methods, time resolution is sacrificed compared with that for femtosecond phase spectroscopy.

In the present paper transform-limited pulses are used in the experiments and assumed for theoretical analyses. However, if femtosecond continuum pulses are used, then the pulse chirp is unavoidable, owing to group-velocity dispersion of optical elements, so the effect of the chirp must be carefully treated. It is important to study dispersion relations measured with chirped pulses and the applicability of the K–K relations to chirp-compensated spectra. These problems will be treated elsewhere.[50]

APPENDIX A

The systematic error that is due to the amplitude change ΔK in relation (15) is estimated as follows. The normalized interference without excitation is expressed from Eq. (3) by

$$F_0(\omega) = 2 + 2\cos\,\omega T\,. \tag{A1}$$

This function has a peak or a valley at $\omega = \omega_0$ when

$$\mathrm{d}F_0(\omega)/\mathrm{d}\omega|_{\omega=\omega_0} = 0\,. \tag{A2}$$

The normalized interference with excitation is expressed, from Eq. (10), by

$$F_{\mathrm{ex}}(\omega) = 1 + \exp(-2\Delta K) + 2\exp(-\Delta K)\cos(\omega T - \Delta\Phi)\,, \tag{A3}$$

where $\Delta\Phi$ is a true phase shift. The measured phase shift $\Delta\Phi_m$ satisfies the following equation:

$$\mathrm{d}F_{\mathrm{ex}}(\omega)/\mathrm{d}\omega = 0 \qquad \text{at} \quad \omega T = \omega_0 T + \Delta\Phi_m\,, \tag{A4}$$

which leads to

$$\mathrm{d}\Delta K/\mathrm{d}\omega[\exp(-\Delta K) + \cos(\omega_0 T + \Delta\Phi_m - \Delta\Phi)] + (T - \mathrm{d}\Delta\Phi/\mathrm{d}\omega)\sin(\omega_0 T + \Delta\Phi_m - \Delta\Phi) = 0\,. \tag{A5}$$

If $|\Delta\Phi - \Delta\Phi_m| \ll 1$, systematic errors are given, from Eq. (A5), by relation (15):

$$\Delta\Phi - \Delta\Phi_m \sim \frac{[1 \pm \exp(-\Delta K)]\mathrm{d}\Delta K/\mathrm{d}\omega}{T - \mathrm{d}\Delta\Phi/\mathrm{d}\omega}\,,$$

where + and − correspond to the cases in which $F_0(\omega)$ has a peak and a valley at $\omega = \omega_0$, respectively.

APPENDIX B

The procedure for deriving averaged phase shifts, shown in Figs. 7 and 12, is as follows. Equations (9) and (10) are composed of three terms that are proportional to $\exp(i\omega t)$ at $t = 0, \pm T$. If

$$F^{-1}[E_{\mathrm{pr}}'(\omega, \tau)] = E_{\mathrm{pr}}'(t)\exp[-\Delta\kappa(t + \tau) + i\Delta\phi(t + \tau)]\,, \tag{B1}$$

where $\Delta\kappa(t)$ and $\Delta\phi(t)$ are proportional to the imaginary and the real parts of the time-dependent complex refractive-index change, respectively, then the inverse FT of the $\exp(-i\omega T)$ term in Eq. (9) is given by

$$\begin{aligned} V(t) &\equiv F^{-1}[E_{\mathrm{pr}}'^{*}(\omega)\exp(-i\omega T)E_{\mathrm{pr}}'(\omega)] \\ &= E_{\mathrm{pr}}'^{*}(t - T) \otimes E_{\mathrm{pr}}'(t)\,. \end{aligned} \tag{B2}$$

Similarly, the inverse FT of the $\exp(-i\omega T)$ term in Eq. (10) is given by

$$\begin{aligned} V(t, \tau) &\equiv F^{-1}\{E_{\mathrm{pr}}'^{*}(\omega)\exp(-i\omega T)E_{\mathrm{pr}}'(\omega) \\ &\quad \times \exp[-\Delta K(\omega, \tau) + i\Delta\Phi(\omega, \tau)]\} \\ &= E_{\mathrm{pr}}'^{*}(t - T) \otimes \{E_{\mathrm{pr}}'(t)\exp[-\Delta\kappa(t + \tau) \\ &\quad + i\Delta\phi(t + \tau)]\} \\ &= V(t)\exp[\Gamma(t, \tau) + i\Psi(t, \tau)]\,, \end{aligned} \tag{B3}$$

where both $\Gamma(t, \tau)$ and $\Psi(t, \tau)$ are real functions. The average changes are obtained by substitution of $t = T$ into Eq. (B3) as

$$\begin{aligned} \Delta K(\tau) &= \Gamma(T, \tau)\,, \\ \Delta\Phi(\tau) &= \Psi(T, \tau)\,, \\ \Delta T/T(\tau) &= [|V(T, \tau)|^2 - |V(T)|^2]/|V(T)|^2 \\ &= \exp[2\Gamma(T, \tau)] - 1\,. \end{aligned} \tag{B4}$$

$\Delta\Phi(\tau)$ in Eqs. (B4) is used for plotting the delay-time dependence of the phase change. This corresponds to the signal obtained by conventional interferometers without a spectrometer as follows: If $\Delta\kappa \ll 1$ and $\Delta\phi \ll 1$ in Eq. (B3), then

$$V(t, \tau) \sim V(t) + V(t)\Gamma(t, \tau) + iV(t)\Psi(t, \tau)\,, \tag{B5}$$

where

$$\begin{aligned} V(t)\Gamma(t, \tau) &= -E_{\mathrm{pr}}'^{*}(t - T) \otimes [E_{\mathrm{pr}}'(t)\Delta\kappa(t + \tau)]\,, \\ V(t)\Psi(t, \tau) &= E_{\mathrm{pr}}'^{*}(t - T) \otimes [E_{\mathrm{pr}}'(t)\Delta\phi(t + \tau)] \\ &= \int \mathrm{d}t' E_{\mathrm{pr}}'^{*}(t - T - t')E_{\mathrm{pr}}'(t')\Delta\phi(t' + \tau)\,. \end{aligned} \tag{B6}$$

If $E_{\mathrm{pr}}'(t)$ is an even function, then

$$\begin{aligned} \Delta\Phi(\tau) &= \Psi(T, \tau) \\ &= \int \mathrm{d}t' E_{\mathrm{pr}}'^{*}(-t')E_{\mathrm{pr}}'(t')\Delta\phi(t' + \tau)/V(T) \\ &= \int \mathrm{d}t|E_{\mathrm{pr}}'(t)|^2\Delta\phi(t + \tau)\Big/\int \mathrm{d}t|E_{\mathrm{pr}}'(t)|^2\,. \end{aligned} \tag{B7}$$

This is exactly the same signal as that obtained by conventional interferometers.

APPENDIX C

Equation (17) is deduced by solution of the optical Bloch equations in a two-level system in the presence of the pump and the probe fields. The third-order perturbation approximation (first order in the probe field and second order in the pump field) yields the level-population, the pump-polarization-coupling, and the PFID terms.[29] The level-population term is expressed by

$$P^{(3)}(t) = \chi^{(3)}(t) \otimes E_{\mathrm{pr}}(t) = 2\mu f_2(t) \otimes [E_{\mathrm{pr}}(t) N^{(2)}(t)], \quad \text{(C1)}$$

where $N^{(2)}(t)$ is the population difference change:

$$N^{(2)}(t) = f_1(t) \otimes [E_{\mathrm{ex}}(t) P_{\mathrm{ex}}^{(1)*}(t) - E_{\mathrm{ex}}{}^{*}(t) P_{\mathrm{ex}}^{(1)}(t)]/2\mu\,; \quad \text{(C2)}$$

$E_{\mathrm{ex}}(t)$ and $E_{\mathrm{pr}}(t)$ are pump and probe fields, given by

$$\begin{aligned} E_{\mathrm{pr}}(t) &= E_1(t)\exp(i\omega_{\mathrm{pr}} t)\,, \\ E_{\mathrm{ex}}(t) &= E_2(t+\tau)\exp[i\omega_{\mathrm{ex}}(t+\tau)]\,; \end{aligned} \quad \text{(C3)}$$

$P_{\mathrm{ex,pr}}^{(1)}(t)$ are pump- and probe-induced polarizations:

$$P_{\mathrm{ex,pr}}^{(1)}(t) = 2\mu N_0 f_2(t) \otimes E_{\mathrm{ex,pr}}(t)\,; \quad \text{(C4)}$$

and $f_1(t)$ and $f_2(t)$ are population- and polarization-response functions:

$$\begin{aligned} f_1(t) &= i(\mu/\hbar)\theta(t)\exp(-t/T_1)\,, \\ f_2(t) &= -(i/2)(\mu/\hbar)\theta(t)\exp[(i\Omega - 1/T_2)t]\,. \end{aligned} \quad \text{(C5)}$$

In Eqs. (C1)–(C5) ω_{ex} and ω_{pr} are pump and probe angular frequencies, μ is the transition dipole moment, N_0 is the equilibrated population difference, T_1 and T_2 are the energy and phase relaxation times, Ω is the transition frequency, and $\theta(t)$ is a normalized step function:

$$\theta(t) = \begin{cases} 1 & t > 0 \\ 0 & t < 0 \end{cases}. \quad \text{(C6)}$$

It is assumed that the pulses are transform limited and have a hyperbolic-secant envelope:

$$E_{1,2}(t) = \mathrm{sech}[2\,\ln(1+\sqrt{2})t/\tau_{\mathrm{pr,ex}}]\,, \quad \text{(C7)}$$

where $\tau_{\mathrm{pr,ex}}$ are the FWHM's of the probe and the pump intensity profiles $I_{\mathrm{pr,ex}}(t) = {E_{1,2}}^2(t)$. From Eqs. (C4) and (C1) we obtain Eqs. (16) and (17):

$$\begin{aligned} \chi^{(1)}(\omega) &= F[P_{\mathrm{pr}}^{(1)}(t)]/E_{\mathrm{pr}}(\omega) = 2\mu N_0 f_2(\omega)\,, \\ \chi^{(3)}(\omega,\tau) &= F[P^{(3)}(t)]/E_{\mathrm{pr}}(\omega) \\ &= 2\mu f_2(\omega) F[E_{\mathrm{pr}}(t) N^{(2)}(t)]/E_{\mathrm{pr}}(\omega)\,. \end{aligned}$$

APPENDIX D

The difference between the present method and conventional time-resolved optical Kerr measurements is described below. The third-order susceptibility is a function of three independent frequencies, $\chi^{(3)}(\omega_1, \omega_2, \omega_3)$. The conventional Kerr measurements give a signal $S(\tau)$ as a function of τ, the time delay between pump and probe pulses with the same central frequency ω_1. Thus $S(\tau)$ is related to the FT of $\chi^{(3)}(\omega_1, \Delta\omega, \omega_1)$ as a function of one variable $\Delta\omega$, where $\Delta\omega = \omega_2 - \omega_1$ is the difference frequency within the pump bandwidth. Femtosecond phase spectroscopy applied to nonresonant Kerr materials gives $S(\omega_1, \tau, \omega)$ or $\chi^{(3)}(\omega_1, \Delta\omega, \omega)$ as a function of two variables, $\Delta\omega$ and ω, where ω is the probe frequency. $S(\omega_1, \tau, \omega)$ shows the dispersion (as a function of ω) of Raman-excited molecules with various (as a function of τ) vibrational displacements or orientational arrangements.

APPENDIX E

In Fig. 16 the K–K relations hold rigorously because both DTS's and DPS's are limited by a finite value to satisfy $\Delta\chi(\omega) \to 0(\omega^{\delta})$ with $\delta \leqq 0$ as $|\omega| \to \infty$. This is proved as follows. Since the probe field $E(t)$ is a single-sided exponential expressed as

$$\begin{aligned} E(t) &= \theta(t)\exp(-Ct)\,, \\ E(\omega) &= F[E(t)] = 1/(i\omega + C)\,, \end{aligned} \quad \text{(E1)}$$

then the polarization change $\Delta P(t)$ is zero for $t < 0$, from Eq. (26). The susceptibility change is expressed as

$$\begin{aligned} \Delta\chi(\omega) &= \int_0^{\infty} \mathrm{d}t\, \exp(-i\omega t)\Delta P(t)/E(\omega) \\ &= \int_0^{\infty} \mathrm{d}t (i\omega + C)\exp(-i\omega t)\Delta P(t) \\ &= G(\omega) + C\Delta P(\omega)\,, \end{aligned} \quad \text{(E2)}$$

where $\Delta P(\omega) = F[\Delta P(t)]$ and

$$\begin{aligned} |G(\omega)| &= \left| \int_0^{\infty} \mathrm{d}t (i\omega)\exp(-i\omega t)\Delta P(t) \right| \\ &\leqq |\Delta P_{\max}[-\exp(-i\omega t)]_0^{\infty}| \leqq |2\Delta P_{\max}|\,. \end{aligned} \quad \text{(E3)}$$

Thus, $\Delta\chi(\omega)$ does not diverge but is limited below a finite value.

Condition C (Subsection 4.E) is the exception for which the weak-probe condition is not necessary. For example, the K–K relations hold for a single-sided exponential pulse $E(t)$ to any order of nonlinearity because, even for $\Delta P(t)$ including $E^n(t)$ for any large n, $\Delta P(t)$ is zero for $t < 0$ and $\Delta\chi(\omega)$ is limited by a finite value, as is known from Eq. (E2) and relations (E3). This is generally true for any pulse that satisfies condition C as follows: The pulse field satisfying condition C can be expressed as $E(t) = \theta(t)f(t)$, where $\theta(t)$ is a step function and $f(t)$ is an arbitrary even function that falls off to zero as $t \to \infty$. Then $E(\omega) = \theta(\omega) \otimes f(\omega)$, where $\theta(\omega) = \lim_{\delta\to+0} \int_0^{\infty} \mathrm{d}t\, \exp(-i\omega t - \delta t) = -i/\omega$. Therefore $E(\omega)$ falls off more slowly than $1/\omega$ as $|\omega| \to \infty$, so that the discussion for Eq. (E2) and relation (E3) is valid for any pulse field that satisfies condition C. From this, the additional condition required for C is only that $1/E(\omega)$ not have poles in the lower half-plane for $|\omega| < \infty$. For example, a rectangular pulse field, defined by

$$E(t) = \begin{cases} 1 & 0 < t < T \\ 0 & t < 0, t > T \end{cases}, \tag{E4}$$

has a spectrum $E(\omega) = i[\exp(-i\omega T) - 1]/\omega$. Since $1/E(\omega)$ has poles at $\omega = 2m\pi/T$ (m is an integer) on the real ω axis, this pulse does not satisfy the additional condition.

ACKNOWLEDGMENTS

This work was carried out at Frontier Research Program, RIKEN (The Institute of Physical and Chemical Research), with the support of A. F. Garito, A. Yamada, H. Sasabe, and T. Wada. The authors express sincere thanks for their support when T. Kobayashi was involved in the program.

*Present address, Institute for Solid State Physics, University of Tokyo, Roppongi 7-22-1, Minato-ku, Tokyo 106, Japan.

†Present address, Department of Chemistry, Faculty of Science, University of Tokyo, 7-3-1 Hongo, Bunkyo-ku, Tokyo 113, Japan.

REFERENCES AND NOTES

1. L. D. Landau and E. M. Lifshitz, *Electrodynamics of Continuous Media* (Addison-Wesley, Reading, Mass., 1960).
2. A. Yariv, *Quantum Electronics*, 3rd ed. (Wiley, New York, 1988).
3. Sh. M. Kogan, Zh. Eksp. Teor. Fiz. **43,** 304 (1962) [Sov. Phys. JETP **16,** 217 (1963)]; P. J. Price, Phys. Rev. **130,** 1792 (1963); W. J. Caspers, Phys. Rev. **133,** A1249 (1964); F. Smet and A. van Groenendael, Phys. Rev. A **19,** 334 (1979); K.-E. Peiponen, Phys. Rev. B **37,** 6463 (1988).
4. F. L. Ridener, Jr., and R. H. Good, Jr., Phys. Rev. B **11,** 2768 (1975); F. Bassani and S. Scandolo, Phys. Rev. B **44,** 8446 (1991).
5. D. A. B. Miller, C. T. Seaton, M. E. Prise, and S. D. Smith, Phys. Rev. Lett. **47,** 197 (1981); D. S. Chemla, D. A. B. Miller, P. W. Smith, A. C. Gossard, and W. Wiegmann, IEEE J. Quantum Electron. **QE-20,** 265 (1984); Y. H. Lee, A. Chavez-Pirson, S. W. Koch, H. M. Gibbs, S. H. Park, J. Morhange, A. Jeffery, N. Peyghambarian, L. Banyai, A. C. Gossard, and W. Wiegmann, Phys. Rev. Lett. **57,** 2446 (1986); J. S. Weiner, D. A. B. Miller, and D. S. Chemla, Appl. Phys. Lett. **50,** 842 (1987); M. A. Fisher, J. Appl. Phys. **67,** 543 (1990); M. Sheik-Bahae, D. C. Hutchings, D. J. Hagen, and E. W. Van Stryland, IEEE J. Quantum Electron. **27,** 1296 (1991).
6. H. Kishida, T. Hasegawa, Y. Iwasa, T. Koda, and Y. Tokura, Phys. Rev. Lett. **70,** 3724 (1993).
7. K. Ichimura, M. Yoshizawa, H. Matsuda, S. Okada, M. M. Ohsugi, H. Nakanishi, and T. Kobayashi, J. Chem. Phys. **99,** 7404 (1993); H. Ooi, M. Yoshizawa, M. Yamashita, and T. Kobayashi, Chem. Phys. Lett. **210,** 384 (1993).
8. E. Tokunaga, A. Terasaki, and T. Kobayashi, Phys. Rev. A **47,** R4581 (1993).
9. J.-M. Halbout and C. L. Tang, Appl. Phys. Lett. **40,** 765 (1982).
10. Y. Li, G. Eichmann, and R. R. Alfano, Appl. Opt. **25,** 209 (1986).
11. H. J. Eichler, P. Günter, and D. W. Pohl, *Laser-Induced Dynamic Gratings* (Springer-Verlag, Berlin, 1986), p. 30.
12. D. Cotter, C. N. Ironside, B. J. Ainslie, and H. P. Girdlestone, Opt. Lett. **14,** 317 (1989).
13. N. Finlayson, W. C. Banyai, C. T. Seaton, G. I. Stegeman, M. O'Neill, T. J. Cullen, and C. N. Ironside, J. Opt. Soc. Am. B **6,** 675 (1989).
14. M. J. LaGasse, K. K. Anderson, H. A. Haus, and J. G. Fujimoto, Appl. Phys. Lett. **54,** 2068 (1989); C. de C. Chamon, C. K. Sun, H. A. Haus, and J. G. Fujimoto, Appl. Phys. Lett. **60,** 533 (1992).
15. K. Minoshima, M. Taiji, and T. Kobayashi, Opt. Lett. **16,** 1683 (1991).
16. G. R. Olbright and N. Peyghambarian, Appl. Phys. Lett. **48,** 1184 (1986).
17. H. Uchiki and T. Kobayashi, J. Appl. Phys. **64,** 2625 (1988).
18. N. Pfeffer, F. Charra, and J. M. Nunzi, Opt. Lett. **16,** 1987 (1991).
19. E. Tokunaga, A. Terasaki, and T. Kobayashi, Opt. Lett. **17,** 1131 (1992).
20. N. F. Scherer, R. J. Carlson, A. Matro, M. Du, A. J. Ruggiero, V. Romero-Rochin, J. A. Cina, G. R. Fleming, and S. A. Rice, J. Chem. Phys. **95,** 1487 (1991).
21. A. Terasaki, M. Hosoda, T. Wada, H. Tada, A. Koma, A. Yamada, H. Sasabe, A. F. Garito, and T. Kobayashi, J. Phys. Chem. **96,** 10534 (1992).
22. Precisely, $E_{\mathrm{ref}}(t) = E(t + T)\exp[i\omega_0(t + T) + i\pi] = -E(t + T)\exp[i\omega_0(t + T)]$ in Eqs. (1) because of the phase shift at the beam splitter. But this modification is equivalent to a slight change of T by π/ω_0, so that the essentials of the following discussion are not affected. For example, Eq. (15) is unchanged. Also, because of the beam splitter's thickness, there is a path difference between the reference and the probe, leading to the chirp difference between the two pulses. But this effect is negligibly small, so it is ignored in Eqs. (1).
23. To compare the transmission change directly with $\Delta\Phi$, it is more appropriate to use $\ln(\Delta T/T)/2 = -\Delta K$ than $\Delta T/T$, especially when ΔK is large. But we use $\Delta T/T$ in this paper because conventionally it has been used most frequently.
24. N. H. Schiller and R. R. Alfano, Opt. Commun. **35,** 451 (1980).
25. M. Tomita, T. Matsumoto, and M. Matsuoka, J. Opt. Soc. Am. B **6,** 165 (1989); M. Tomita and M. Matsuoka, J. Opt. Soc. Am. B **7,** 1198 (1990).
26. C. H. Brito-Cruz, R. L. Fork, W. H. Knox, and C. V. Shank, Chem. Phys. Lett. **132,** 341 (1986).
27. B. Fluegel, N. Peyghambarian, G. Olbright, M. Lindberg, S. W. Koch, M. Joffre, D. Hulin, A. Migus, and A. Antonetti, Phys. Rev. Lett. **59,** 2588 (1987); J. P. Sokoloff, M. Joffre, B. Fluegel, D. Hulin, M. Lindberg, S. W. Koch, A. Migus, A. Antonetti, and N. Peyghambarian, Phys. Rev. B **38,** 7615 (1988).
28. M. Lindberg and S. W. Koch, J. Opt. Soc. Am. B **5,** 139 (1988); Phys. Rev. B **38,** 7607 (1988).
29. C. H. Brito-Cruz, J. P. Gordon, P. C. Becker, R. L. Fork, and C. V. Shank, IEEE J. Quantum Electron. **24,** 261 (1988).
30. M. Joffre, D. Hulin, A. Migus, A. Antonetti, C. Benoit a la Guillaume, N. Peyghambarian, M. Lindberg, and S. W. Koch, Opt. Lett. **13,** 276 (1988); M. Joffre, D. Hulin, A. Migus, and A. Antonetti, J. Mod. Opt. **35,** 1951 (1988); M. Joffre, D. Hulin, J.-P. Foing, J.-P. Chambaret, A. Migus, and A. Antonetti, IEEE J. Quantum Electron. **25,** 2505 (1989).
31. R. R. Alfano and P. P. Ho, IEEE J. Quantum Electron. **QE-24,** 351 (1988).
32. W. M. Wood, G. Focht, and M. C. Downer, Opt. Lett. **13,** 984 (1988); M. C. Downer, W. M. Wood, and J. I. Trisnadi, Phys. Rev. Lett. **65,** 2832 (1990).
33. T. Hattori, A. Terasaki, T. Kobayashi, T. Wada, A. Yamada, and H. Sasabe, J. Chem. Phys. **95,** 937 (1991).
34. E. Tokunaga, A. Terasaki, T. Wada, K. Tsunetomo, Y. Osaka, and T. Kobayashi, J. Opt. Soc. Am. B **10,** 2364 (1993).
35. From Eq. (29) it follows that for a two-level system the real and the imaginary parts of $\Delta\chi(\omega)$ show the same dynamics as a function of τ for all ω's. The assumption of the two-level system in Subsection 3.A is based on this equation.
36. A. Nakamura and T. Tokizaki, Solid State Phys. **24,** 931 (1989).
37. $\Delta\Phi(\tau)$ of Fig. 3 of Ref. 8 shows a less sharp peak near zero delay than the present result in Fig. 12. This is because $\Delta\Phi(\tau) = \int_{T-\Delta T}^{T+\Delta T} \mathrm{d}t\Psi(t, \tau)$ was used previously instead of $\Delta\Phi(\tau) = \Psi(T, \tau)$, in Eqs. (B4) used here.
38. J. Etchepare, G. Grillon, J.-P. Chambaret, G. Hamoniaux, and A. Orszag, Opt. Commun. **63,** 329 (1987).
39. C. Kalpouzos, D. McMorrow, W. T. Lotshaw, and G. A. Kenney-Wallace, Chem. Phys. Lett. **150,** 138 (1988); Comment Chem. Phys. Lett. **155,** 240 (1989).

40. S. Ruhman and K. A. Nelson, J. Chem. Phys. **94,** 859 (1991).
41. T. Hattori and T. Kobayashi, J. Chem. Phys. **94,** 3332 (1991).
42. R. L. Fork, C. V. Shank, C. Hirlimann, R. Yen, and W. J. Tomlinson, Opt. Lett. **8,** 1 (1983).
43. R. R. Alfano, ed. *The Supercontinuum Laser Source* (Springer-Verlag, New York, 1989).
44. D. McMorrow and W. T. Lotshaw, Chem. Phys. Lett. **174,** 85 (1990).
45. Y.-X. Yan and K. A. Nelson, J. Chem. Phys. **87,** 6257 (1987).
46. H. A. Haus, IEEE J. Quantum Electron. **QE-11,** 736 (1975).
47. To be strict, the results at the left and the right in the middle of Fig. 15 also do not satisfy the K–K relations, because they diverge to infinity as $|\omega| \rightarrow \infty$, although conditions B are strictly satisfied together with the additional conditions because a hyperbolic-secant envelope is assumed for $E(\omega)$. This means that the additional conditions are not sufficient but only necessary conditions.
48. The chirped-pulse case is discussed in Refs. 49 and 50.
49. E. Tokunaga, A. Terasaki, and T. Kobayashi, Opt. Lett. **18,** 370 (1993).
50. E. Tokunaga, A. Terasaki, and T. Kobayashi, "Femtosecond continuum interferometer for transient phase and transmission spectroscopy," submitted to J. Opt. Soc. Am. B.
51. A. Miller, D. A. B. Miller, and S. D. Smith, Adv. Phys. **30,** 697 (1981).
52. E. Tokunaga, A. Terasaki, V. Valencia, T. Wada, H. Sasabe, and T. Kobayashi, "Femtosecond phase spectroscopy of multi-level systems: phthalocyanines," submitted to J. Opt. Soc. Am. B.